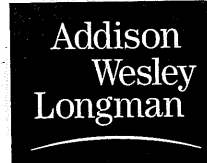


SECOND EDITION

MECHANICS AND THERMODYNAMICS OF PROPULSION

PHILIP G. HILL
University of British Columbia

CARL R. PETERSON
Massachusetts Institute of Technology



ADDISON-WESLEY PUBLISHING COMPANY
Reading, Massachusetts ■ Menlo Park, California ■ New York
Don Mills, Ontario ■ Wokingham, England ■ Amsterdam ■ Bonn
Sydney ■ Singapore ■ Tokyo ■ Madrid ■ San Juan ■ Milan ■ Paris

AXIAL TURBINES

8.1 INTRODUCTION

Turbines, like compressors, can be classified into radial, axial, and mixed-flow machines. In the axial machine the fluid moves essentially in the axial direction through the rotor. In the radial type the fluid motion is mostly radial. The mixed-flow machine is characterized by a combination of axial and radial motion of the fluid relative to the rotor. The choice of turbine type depends on the application, though it is not always clear that any one type is superior.

Comparing axial and radial turbines of the same overall diameter, we may say that the axial machine, just as in the case of compressors, is capable of handling considerably greater mass flow. On the other hand, for small mass flows the radial machine can be made more efficient than the axial one. The radial turbine is capable of a higher pressure ratio per stage than the axial one. However, multi-staging is very much easier to arrange with the axial turbine, so that large overall pressure ratios are not difficult to obtain with axial turbines.

In order to minimize the turbojet engine nacelle drag and the engine weight per unit thrust, the mass flow per unit cross-sectional area must be as large as possible. The limiting mass flow of turbojet engines depends mainly on the maximum permissible Mach number of the flow entering the compressor. It is generally large enough to require the mass flow capability of an axial turbine, even with engines that have centrifugal (radial flow) compressors. Thus the following study concerns axial turbines only.

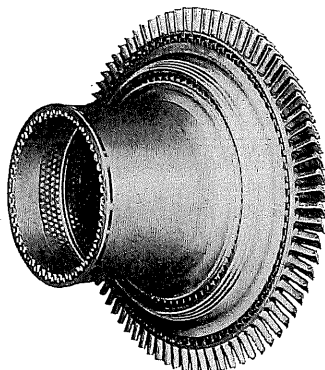


FIGURE 8.1 High-pressure turbine rotor for the CFM56 engine. (Courtesy GE Aircraft Engines.)

Generally the efficiency of a well-designed turbine is higher than the efficiency of a compressor. Moreover, the design process is somewhat simpler. The principal reason for this fact is that the fluid undergoes a pressure *drop* in the turbine and a pressure *rise* in the compressor. The pressure drop in the turbine is sufficient to keep the boundary layer fluid generally well behaved, and separation problems that are often serious in compressors can be relatively easily avoided. Offsetting this advantage is the much more critical stress problem, since turbine rotors must operate in very high temperature gas. Actual blade shape is often more dependent on stress and cooling considerations than on aerodynamic considerations, beyond the satisfaction of the velocity-triangle requirements.

Because of the generally falling pressure in turbine flow passages, much more turning in a given blade row is possible without danger of flow separation than in an axial compressor blade row. This means much more work, and considerably higher pressure ratio, per stage.

In recent years advances have been made in turbine blade cooling and in the metallurgy of turbine blade materials. This means that turbines are able to operate successfully at increasingly high inlet gas temperatures and that substantial improvements are being made in turbine engine thrust, weight, and fuel consumption.

By way of illustration, Fig. 8.1 presents the high-pressure turbine rotor for the CFM56 engine[†] (shown in Fig. 5.24). Figure 8.2 is a photograph of the blades showing the “fir tree” root geometry and the holes in the blade surface from which cooling air emerges to shield the blade from the high-temperature gas. Small tip clearances are needed for high turbine efficiency. Note that there is a recessed region at the tip of the blade; an accidental “rub” of the blade tip on the turbine casing is not nearly as serious with a recessed tip as with a blade that has a full cross section at the tip diameter. Figure 8.1 shows that the hub–tip ratio for

[†] Produced by CFM International, a joint company of GE Aircraft Engines and Société Nationale d'Etude et de construction de Moteurs d'Aviation.

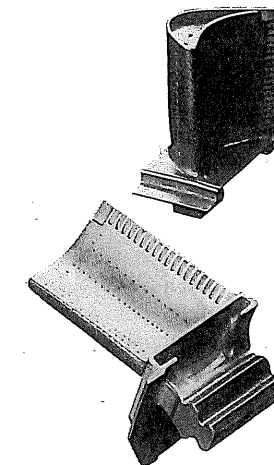


FIGURE 8.2 High-pressure turbine rotor blades for the CFM56 engine. (Courtesy GE Aircraft Engines.)

this turbine is quite high. Thus very little blade twist is required for the blade to match the radial variations in gas velocity and wheel speed. Low-pressure turbines (handling low-density gas) will typically have a much lower hub–tip ratio and a larger blade twist.

Figure 8.3 shows the stator or “nozzle” blades that feed swirling high-velocity gas to the turbine rotor. These too are cooled by a flow of high-pressure air from the compressor that passes through each stator blade, exhausting through a pat-

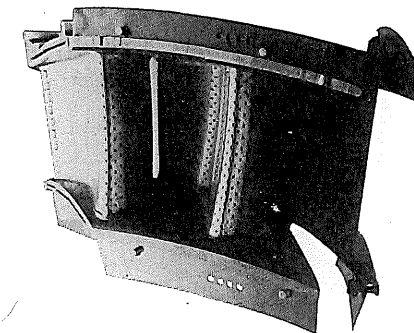


FIGURE 8.3 High-pressure turbine stator blades for the CFM56 engine. (Courtesy GE Aircraft Engines.)

tern of small holes in the blade surface. We will address the subject of film cooling of the blades later in this chapter.

8.2 THE AXIAL TURBINE STAGE

An axial turbine stage consists of a row of stationary blades, called nozzles or stators, followed by the rotor, as Fig. 8.4 illustrates. Because of the large pressure drop per stage, the nozzle and rotor blades may be of increasing length, as shown, to accommodate the rapidly expanding gases, while holding the axial velocity to something like a uniform value through the stage.

A section through the mean radius would appear as in Fig. 8.5. One can see that the nozzles accelerate the flow, imparting an increased tangential velocity component. The velocity diagram of the turbine differs from that of the compressor in that the change in tangential velocity in the rotor, Δc_θ , is in the direction opposite to the blade speed U . The reaction to this change in the tangential momentum of the fluid is a torque on the rotor in the direction of motion. Hence the fluid does work on the rotor. Again applying the angular momentum relationship as in Eq. (7.8), we may show that the power output is

$$\mathcal{P} = \dot{m}(U_2 c_{\theta 2} - U_3 c_{\theta 3}). \quad (8.1)$$

In an axial turbine, $U_2 \approx U_3 = U$. The turbine work per unit mass is

$$W_T = U(c_{\theta 2} - c_{\theta 3}) \quad \text{or} \quad W_T = c_p(T_{01} - T_{03}).$$

Defining

$$\Delta T_0 = T_{01} - T_{03} = T_{02} - T_{03},$$

we find that the stage work ratio is

$$\frac{\Delta T_0}{T_{01}} = \frac{U(c_{\theta 2} - c_{\theta 3})}{c_p T_{01}}. \quad (8.2)$$

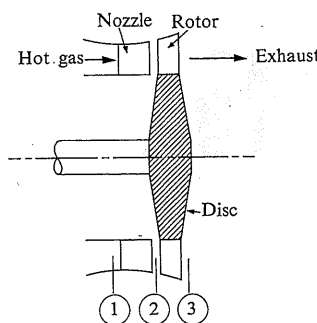


FIGURE 8.4 An axial turbine stage.

8.2 THE AXIAL TURBINE STAGE

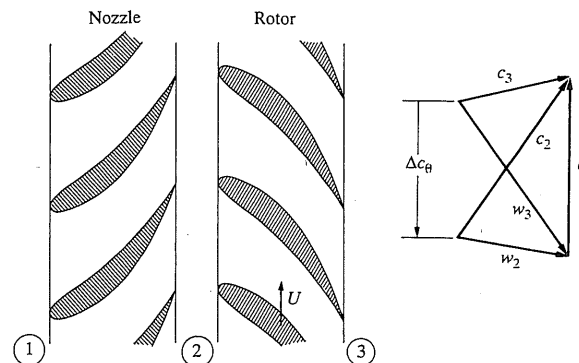


FIGURE 8.5 Turbine blading and velocity triangles.

In considering the possibility of maximizing the turbine work per stage, we can see that the work may be limited in one of two ways: (1) The available pressure ratio (and thus $\Delta T_0/T_{01}$) may be limited. In this case the maximum work will be directly proportional to T_{01} . (2) The available pressure ratio may be sufficiently high that the work will be limited by the allowable blade speed U and the allowable turning Δc_θ of the fluid. Blade speed is limited by the allowable rotational stresses at the operating temperature, while Δc_θ must be limited to maintain high efficiency. The allowable turning in a turbine stage is much higher than in a compressor stage, but the turning must not be too large if the turbine is to be highly efficient.

Boundary layers in turbines tend to be well behaved because of the generally falling pressure gradient. Figure 8.6 indicates that the greater the acceleration—that is, the larger the pressure drop—in a given blade row, the smaller the losses. If, perhaps during off-design operation, a part of the flow passage were loaded with decelerating flow, losses could rise considerably.

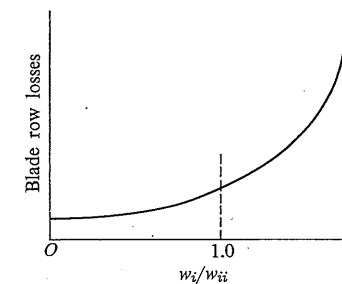


FIGURE 8.6 Turbine blade row losses.

Even though the pressure may be generally falling within a blade passage, locally (on the suction surface of the blade) there could be a zone of adverse gradient, depending on the turning and on the spacing of the blades. Thus boundary layers could grow rapidly or even separate in such a region, with adverse effect on turbine efficiency.

Instead of using the temperature-drop ratio given by Eq. (8.2), turbine designers generally refer to the turbine work ratio that is defined by

$$\frac{W_T}{U^2} = \frac{\Delta h_0}{U^2} = \frac{c_{\theta 2} - c_{\theta 3}}{U}. \quad (8.3)$$

The boundary layer limitation on compressor blading points to the desirability of approximately equal pressure change per blade row. Turbine blade row performance is not nearly so sensitive to the condition of the boundary layer (as long as the pressure is not rising through the passage). Thus the turbine designer has considerably more freedom to distribute the total stage pressure drop between rotor and stator.

Stage Dynamics and Degree of Reaction

Turbine stages in which the entire pressure drop occurs in the nozzle are called *impulse stages*. Stages in which a portion of the pressure drop occurs in the nozzle and the rest in the rotor are called *reaction stages*.

The degree of reaction may be defined for a turbine as the fraction of overall enthalpy drop occurring in the rotor. If in the rotor the enthalpy is constant, the pressure would ideally be constant also. An impulse turbine would therefore be a zero reaction machine. In a 50% reaction machine, the enthalpy drop in the rotor would be half of the total for the stage.

An impulse turbine stage is shown in Fig. 8.7, along with a typical diagram for the common case of constant axial velocity. Since no enthalpy change occurs within the rotor, the energy equation within the rotor requires that $|w_2| = |w_3|$. If the axial velocity component is held constant, then this requirement is satisfied by

$$\beta_3 = -\beta_2.$$

The effect of nozzle outlet angle on impulse turbine work can be seen by transforming Eq. (8.3) as follows: From the velocity diagram we can see that

$$w_{\theta 3} = -w_{\theta 2}$$

and that

$$c_{\theta 2} - c_{\theta 3} = 2w_{\theta 2} = 2(c_{\theta 2} - U),$$

so that

$$c_{\theta 2} - c_{\theta 3} = 2U \left(\frac{c_z}{U} \tan \alpha_2 - 1 \right).$$

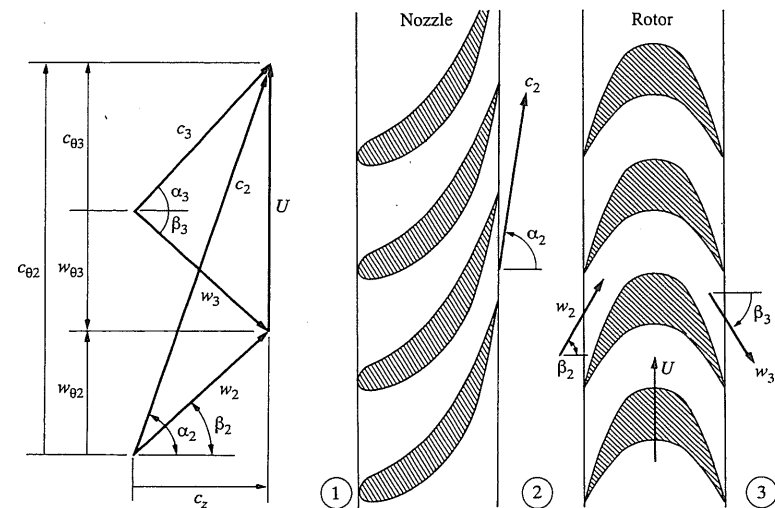


FIGURE 8.7 Impulse turbine stage and constant axial velocity.

Thus we can write Eq. (8.3) as

$$\frac{\Delta h_0}{U^2} = 2 \left(\frac{c_z}{U} \tan \alpha_2 - 1 \right). \quad (8.4)$$

It is evident, then, that for large power output the nozzle angle should be as large as possible. Two difficulties are associated with very large α_2 . For reasonable axial velocities (i.e., reasonable flow per unit frontal area), it is evident that large α_2 creates very large absolute and relative velocities throughout the stage. High losses are associated with such velocities, especially if the relative velocity w_2 is supersonic. In practice, losses seem to be minimized for values of α_2 around 70°. In addition, one can see that for large α_2 [$\tan \alpha_2 > (2U/c_z)$], the absolute exhaust velocity will have a swirl in the direction opposite to U . While we have not introduced the definition of turbine efficiency as yet, it is clear that, in a turbojet engine where large *axial* exhaust velocity is desired, the kinetic energy associated with the tangential motion of the exhaust gases is essentially a loss. Furthermore, application of the angular momentum equation over the entire engine indicates that exhaust swirl is associated with an (undesirable) net torque acting on the aircraft. Thus the desire is for axial or near-axial absolute exhaust velocity (at least for the last stage if a multistage turbine is used). For the special case of constant c_z and axial exhaust velocity, $c_{\theta 3} = 0$ and $c_{\theta 2} = 2U$. So Eq. (8.2) becomes

$$\frac{\Delta h_0}{U^2} = 2. \quad (8.5)$$

For a given power and rotor speed, and for a given peak temperature, Eq. (8.4) is sufficient to determine approximately the mean blade speed (and hence radius) of a single-stage impulse turbine having axial outlet velocity. If, as is usually the case, the blade speed is too high (for stress limitations), or if the mean diameter is too large relative to the other engine components, it is necessary to employ a multistage turbine in which each stage does part of the work.

If the ratio of blade length to mean radius is small, this mean-radius analysis is sufficient for the entire blade length. If the blade is relatively long, however, one should consider radial variations; and we will see that impulse design at the mean radius may lead to difficulty at the hub. We saw previously that the 50% reaction compressor stage (with constant c_z) has symmetrical velocity triangles. The same is true for the 50% reaction turbine stage. Since the changes in static enthalpy are the same in both blade rows, the change in kinetic energy relative to each blade row must be the same. Thus for constant axial velocity, the velocity triangles are as shown in Fig. 8.8. Since the diagram is symmetrical,

$$c_{\theta 3} = -(c_z \tan \alpha_2 - U)$$

for constant axial velocity. Therefore Eq. (8.2) for this case becomes

$$\frac{\Delta h_0}{U^2} = \left(2 \frac{c_z}{U} \tan \alpha_2 - 1 \right). \quad (8.6)$$

Again the desirability of large α_2 is indicated and the same limitations are encountered, so that typical values of α_2 are near 70°. For the special case of axial

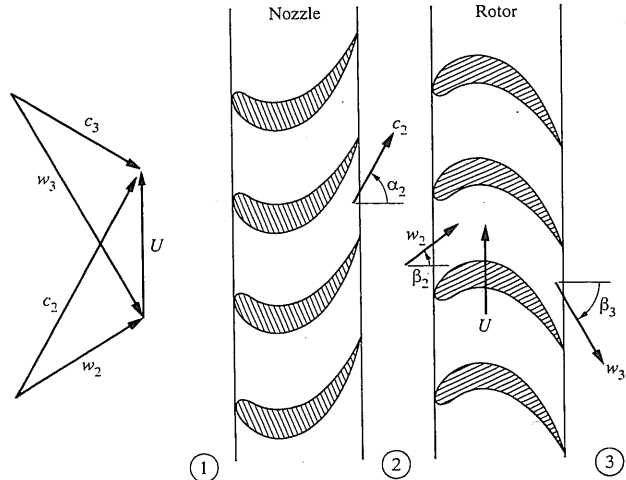


FIGURE 8.8 Fifty-percent reaction blading and constant axial velocity.

outlet velocity and constant c_z , α_3 and β_2 are zero and the velocity diagram becomes a rectangle. The stage work output is then

$$\frac{\Delta h_0}{U^2} = 1. \quad (8.7)$$

Thus, for the same blade speed and for axial outlet velocities, the impulse stage work is twice that of the 50% reaction stage. We can expect the impulse stage to have somewhat greater loss, however, since the average fluid velocity in the stage is higher and since the boundary layer on the suction side of the rotor blades may be significantly thicker and closer to separation, depending on the turning angle and blade spacing.

The 50% reaction stage is not uniquely desirable, of course. One can use any degree of reaction (greater than zero) to design a turbine of acceptable performance. As we will see, the mean-radius velocity triangles may be largely dependent on radial variations and problems encountered near the hub.

For the special case of axial turbines designed for a given stator exit flow angle, and for zero exit swirl, the stage work ratio, defined as $W_T/U^2 = \Delta h_0/U^2$, and the degree of reaction R , depend on flow coefficient, as shown in Fig. 8.9. Here, for zero exit swirl,

$$W_T = \Delta h_0 = U c_{\theta 2} = U c_z \tan \alpha_2,$$

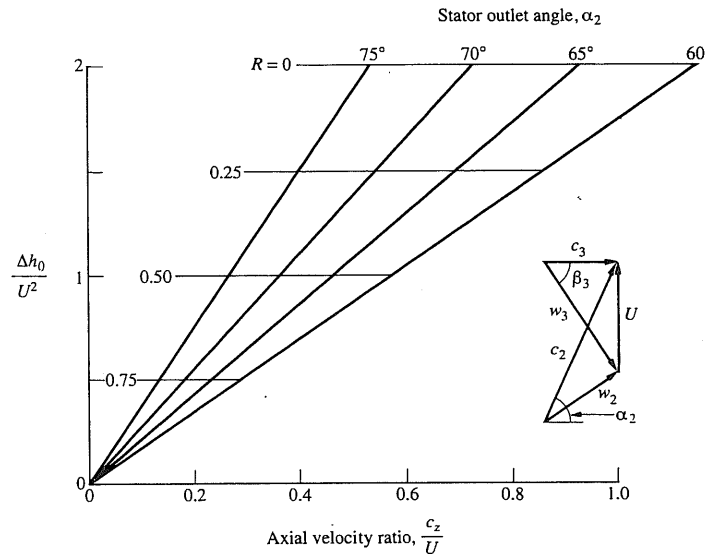


FIGURE 8.9 Work ratio $\Delta h_0/U^2$ and degree of reaction R of axial turbine stages designed for zero exit swirl.

so

$$\frac{\Delta h_0}{U^2} = \frac{c_z}{U} \tan \alpha_2. \quad (8.8)$$

We can define the degree of reaction for axial turbines (with reference to Fig. 8.5) as

$$R = \frac{h_2 - h_3}{h_{01} - h_{03}}. \quad (8.9)$$

Since, in a coordinate system fixed to the rotor, the apparent stagnation enthalpy is constant,

$$h_2 - h_3 = \frac{w_2^2}{2} - \frac{w_3^2}{2}.$$

If the axial velocity is the same upstream and downstream of the rotor, this becomes

$$h_2 - h_3 = \frac{1}{2}(w_{\theta3}^2 - w_{\theta2}^2) = \frac{1}{2}(w_{\theta3} - w_{\theta2})(w_{\theta3} + w_{\theta2}).$$

Also, since $h_{01} - h_{03} = U(c_{\theta2} - c_{\theta3})$, we can write the degree of reaction as

$$R = \frac{(w_{\theta3} - w_{\theta2})(w_{\theta3} + w_{\theta2})}{2U(c_{\theta2} - c_{\theta3})}.$$

But since $w_{\theta3} - w_{\theta2} = c_{\theta3} - c_{\theta2}$, we find

$$R = -\frac{w_{\theta3} + w_{\theta2}}{2U}.$$

For constant axial velocity we can write

$$w_{\theta3} = c_z \tan \beta_3$$

and

$$w_{\theta2} = c_z \tan \alpha_2 - U,$$

so that

$$R = \frac{1}{2} \left[1 - \frac{c_z}{U} (\tan \alpha_2 + \tan \beta_3) \right]. \quad (8.10)$$

Equation (8.10) is a general result. For the special case of symmetrical triangles ($\alpha_2 = -\beta_3$), we have $R = 1/2$. For the case $w_{\theta3} = -w_{\theta2}$ we have $R = 0$. For the special case $c_{\theta3} = 0$ it follows that $w_{\theta3} = c_z \tan \beta_3 = -U$, so that the degree of reaction becomes

$$R = 1 - \frac{1}{2} \left(\frac{c_z}{U} \right) \tan \alpha_2. \quad (8.11)$$

Equations (8.8) and (8.11) have been used in plotting Fig. 8.9, which pertains to design conditions only. Here we see that for a given stator outlet angle, the im-

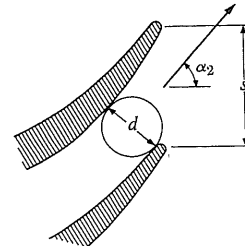


FIGURE 8.10 Flow at nozzle exit.

pulse stage requires a much higher axial velocity ratio than does the 50% reaction stage. In the impulse stage all flow velocities are higher, and that is one reason why its efficiency is lower than that of the 50% reaction stage.

Deviation

The flow at the exit of a turbine rotor or nozzle blade, just as is the case in compressors, does not leave at exactly the blade exit angle. However, the generally well-behaved flow in a turbine blade row, unlike compressor behavior, is more amenable to simple correlations.

Figure 8.10 shows the conditions between two turbine blades. It has been found by experience that the actual exit flow angle at the design pressure ratio of the machine is fairly well approximated by $\alpha_2 = \cos^{-1}(d/s)$, so long as the nozzle is not choked. If the nozzle is choked, then a supersonic expansion may take place at the blade exit and alter the flow direction, providing the exit pressure is sufficiently low.

Figure 8.11 shows a schlieren photograph of such an expansion for a two-dimensional flow through a cascade of blades representing a rotor with 130° of turning and an isentropic outlet Mach number of 1.15. The blade-chord Reynolds number is 7×10^5 . For cooling and structural integrity the blade thickness at each "trailing edge" has finite thickness. An oblique shock leaving the trailing edge on the pressure side of the blade intersects with the boundary layer on the suction surface of the opposite blade. The shock-boundary layer interaction and reflected shock are both visible in Fig. 8.11; so is the thickness of the blade wake region.

8.3 STAGE EFFICIENCY

As the preceding implies, aerodynamic losses in the turbine differ with the stage configuration, that is, the degree of reaction. Improved efficiency is associated with higher reaction, which tends to mean less work per stage and thus a larger number of stages for a given overall pressure ratio.

The understanding of aerodynamic losses is important to design, not only in the choice of blading type (impulse or reaction) but also in devising ways to

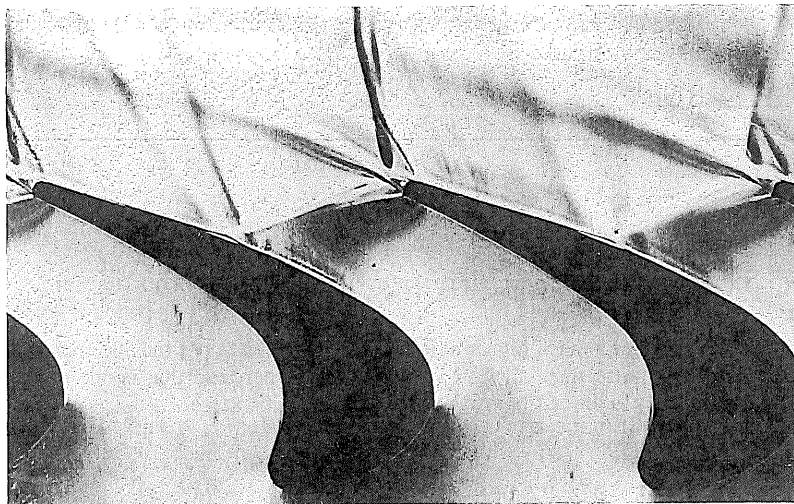


FIGURE 8.11 Schlieren visualization of flow through a linear cascade of high-pressure transonic turbine rotor blades (130° turning). A three-color filter was aligned with the suction surface to show details of the shock-laminar boundary layer interaction. The characteristic "travelling" shocks separated by an expansion are clearly visible. Transition occurs on reattachment of the separation bubble. The isentropic outlet Mach number is 1.15, and the Reynolds number is 7×10^5 (based on chord). (Photo by J. J. Camus, Whittle Laboratory, Cambridge, from a research program sponsored by Rolls-Royce.)

control these losses, for example, methods to control the clearance between the tip of the turbine blade and the outer casing wall. The choices of blade shape, aspect ratio, spacing, Reynolds number, Mach number, and flow incidence angle can all affect the losses and hence the efficiency of turbine stages. To describe the actual process of expansion in a turbine, and thus be able to relate work output to fluid pressure, it is convenient to define an ideal expansion that is reversible and to relate the actual expansion to the ideal through an empirical efficiency. The actual turbine work is expressed in Eq. (8.2) as the drop in stagnation enthalpy $\Delta h_0 = c_p \Delta T_0$. Since even high-temperature turbines are essentially adiabatic devices, the ideal turbine would be an isentropic one. The relationships we will define between actual and ideal processes are shown in the $T-s$ diagram of Fig. 8.12.

Efficiency Definitions

Two turbine efficiencies are in common usage; the choice between them depends on the application for which the turbine is used. For many conventional turbine applications, useful turbine output is in the form of shaft power and ex-

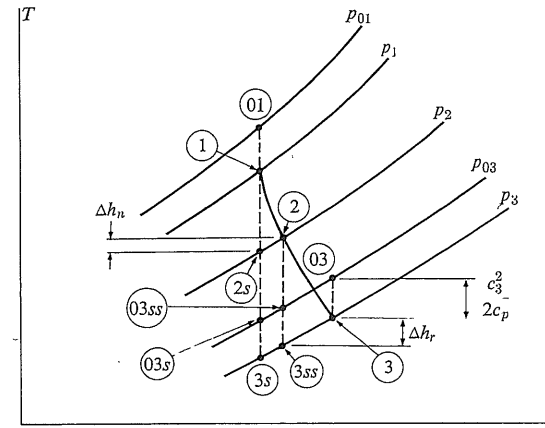


FIGURE 8.12 Expansion in a turbine.

haust kinetic energy, $c_3^2/2$, is considered a loss. In this case the ideal turbine would be an isentropic machine with no exhaust kinetic energy, and

$$W_{T,\text{ideal}} = c_p(T_{01} - T_{3s}).$$

If the actual turbine work is compared with this ideal work, the efficiency is called *total-to-static turbine efficiency*, since the ideal work is based on total (or stagnation) inlet conditions and static exit pressure.

The total-to-static turbine efficiency η_{ts} is defined by

$$\eta_{ts} = \frac{T_{01} - T_{03}}{T_{01} - T_{3s}},$$

or

$$\eta_{ts} = \frac{T_{01} - T_{03}}{T_{01}[1 - (p_3/p_{01})^{(\gamma-1)/\gamma}]} = \frac{1 - (T_{03}/T_{01})}{1 - (p_3/p_{01})^{(\gamma-1)/\gamma}}. \quad (8.12)$$

In some applications, particularly turbojets, the exhaust kinetic energy is not considered a loss since the exhaust gases are intended to emerge at high velocity. The ideal work in this case is then $c_p(T_{01} - T_{03s})$ rather than $c_p(T_{01} - T_{3s})$. This requires a different definition of efficiency, the *total-to-total turbine efficiency* η_{tt} , defined by

$$\eta_{tt} = \frac{T_{01} - T_{03}}{T_{01} - T_{03s}} = \frac{1 - (T_{03}/T_{01})}{1 - (p_{03}/p_{01})^{(\gamma-1)/\gamma}}. \quad (8.13)$$

It is this latter efficiency that is of most interest for turbojet turbines. We may compare the two by making the approximation (see Fig. 8.12) that

$$T_{03s} - T_{3s} \approx T_{03} - T_3 = c_3^2/2c_p,$$

and using Eqs. (8.12) and (8.13) to show that

$$\eta_{tt} = \frac{\eta_{ts}}{1 - c_3^2[2c_p(T_{01} - T_{3s})]}.$$

Thus

$$\eta_{tt} > \eta_{ts}.$$

Regardless of these definitions, the energy associated with the *tangential component* of the turbine exhaust velocity must be considered a loss, since it will not be transformed to axially directed momentum at the exit of the turbojet exhaust nozzle. These definitions also serve for multistage turbines. If the states ① and ③ correspond to inlet and outlet, respectively, we may write the actual turbine work as

$$w_t = \eta_{tt} c_p T_{01} \left[1 - \left(\frac{p_{03}}{p_{01}} \right)^{(y-1)/y} \right].$$

or

$$w_t = \eta_{ts} c_p T_{01} \left[1 - \left(\frac{p_3}{p_{01}} \right)^{(y-1)/y} \right].$$

The difficulties in predicting the efficiency of a turbine stage are comparable to those discussed for compressor stages in Chapter 7. However, it appears that experimental results for the efficiency of well-designed turbines can be correlated quite well with stage work ratio and axial velocity ratio.

In designing a turbine for high efficiency, one of the important questions is how widely spaced the turbine blades should be. Close spacing of blades means large total surface area, numerous blade surface boundary layers, and plentiful opportunity for viscous dissipation both in the boundary layers and in the "wake" mixing regions downstream of the blades. If the blades are widely spaced, the number of boundary layers and wakes is less, but the total force exerted by each blade on the flow must be large (for a given total torque). Larger blade force necessarily means larger pressure difference between suction and pressure surfaces and, in particular, more danger of adverse pressure gradient (on the suction surface between the minimum pressure point and the trailing edge). As we mentioned earlier, such an adverse gradient could lead to large boundary layer growth (even to flow separation) and larger viscous losses. These considerations indicate that there will be an optimum spacing. In the light of lengthy historical experience, turbine designers are widely agreed that this optimum can be determined by using the criterion first devised by Zweifel in the form of a blade force coefficient Z , which is defined as

$$Z = \frac{F_\theta}{(p_{0i} - p_{ii})b_z}.$$

Here F_θ is the tangential component of blade force (per unit blade height) and b_z is the width of the blade row in the axial direction; p_{0i} is the stagnation pressure

at entrance to the blade row, and p_{ii} is the static pressure at exit. If the flow were incompressible, with the same axial velocity component upstream and downstream of the blade row, we could write the force coefficient (see Problem 8.16) as:

$$Z = 2 \frac{s}{b_z} \cos^2 \beta_{ii} (\tan \beta_i - \tan \beta_{ii}). \quad (8.14)$$

Though this expression was originally derived for incompressible flow, it has been found that even with compressible flow the optimum blade spacing can be obtained from Eq. (8.14) by setting $Z = 0.8$. In these pages we are discussing the efficiency of axial turbines whose blade spacing is governed by approximately this value of Z .

The efficiency that a well-designed turbine stage may achieve depends quite strongly on the stage work and flow coefficients $\Delta h_0/U^2$ and c_z/U . Figure 8.13 shows the correlation of Kacker and Okapuu [1], a modification of the earlier work of Smith [2], who plotted the total-to-total efficiencies of some 69 turbines against design axial velocity ratio, showing a point for each design value of the work ratio. The experimental numbers were "corrected" to correspond to zero tip leakage, then the contours shown in Fig. 8.13 were drawn with the guidance of the adjusted experimental data. These provide a good general indication of what to expect for the efficiency of typical gas turbines (except for allowing for tip clearance loss).

Figure 8.13 indicates that if the stage work is kept low enough (and if tip clearance losses are kept to 1% or 2%), the axial turbine stage efficiency can be

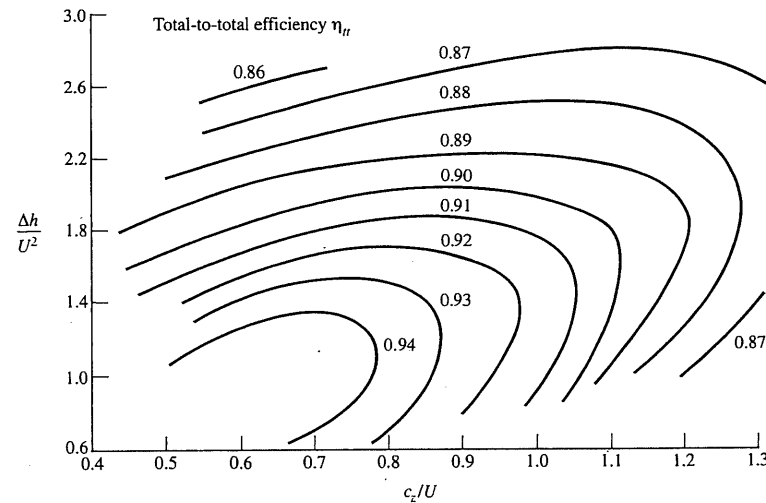


FIGURE 8.13 Turbine stage efficiency at zero tip leakage calculated by the method of Kacker and Okapuu [1].

as high as 92% or 93%. The graph shows that for maximum efficiency $\Delta h_0/U^2$ should not be much greater than 1 and that the axial velocity ratio should be around 0.6 or 0.7. If the turbine were designed for zero exit swirl, Fig. 8.9 suggests that under these conditions the degree of reaction would be of the order of 0.5 and the stator outlet angle would be considerably less than maximum (possibly less than 60°). In aircraft turbine engines the typical efficiency is appreciably less than maximum because of the need to increase stage work ratios to reduce the number of stages and the weight of the turbine. A severe test of the effect of high stage loading has been reported by Moustapha, Okapuu, and Williamson [3]. They built three turbine stages with pressure ratio 3.76, stage work parameter $\Delta h_0/U^2 = 2.47$, and axial velocity ratio at the mean radius of 0.64. The stage efficiency exceeded 80%.

Much work has been done in the past fifty years to correlate the various sources of loss on gas and steam turbines. Intensive reviews of this subject have been prepared by Horlock [4], Denton [5], Gregory-Smith [6], and Sieverding [7]. One of the most widely used methods of performance prediction is that of Ainley and Mathieson, as modified by Dunham and Came [8]. Unfortunately there are considerable disagreements among various empirical loss-correlation methods, and Sieverding concludes his survey by remarking: "The clearance flow mechanism and its effect on the total flow field are still far from being understood. Aerodynamic parameters such as blade load distribution, Mach number and coolant ejection from the blade tip, and geometric configurations such as partial shrouds and recessed casings for unshrouded blades will need attention in the future."

With this in mind we return to the Denton-Cumpsty framework [9] for discussion of entropy generation in turbomachines. For a turbine with stagnation pressure ratio p_{04}/p_{05} , we may write the total-to-total efficiency as

$$\eta_{tt} = \frac{h_{04} - h_{05}}{h_{04} - h_{05s}}$$

or, with constant specific-heat ratio,

$$\eta_{tt} = \frac{1 - \left(\frac{p_{05}}{p_{04}}\right)^{(\gamma-1)/\gamma} e^{\Delta s/c_p}}{1 - \left(\frac{p_{05}}{p_{04}}\right)^{(\gamma-1)/\gamma}}, \quad (8.15)$$

so that if we know the total entropy generation Δs per unit mass of working fluid, we can determine the adiabatic efficiency. The assumptions made for entropy generation in boundary layers are appropriate for turbines as well as for compressors, so that for turbine blades also we may estimate the entropy generation rate per unit area of turbine blade surface by using Eq. (7.36).

In general the same considerations apply (for turbines and compressors) to entropy generation in blade wakes and at end walls. But, there are at least four

qualitative differences: First, for unshrouded blades[†] the stationary casing acts more strongly to promote cross-flow in the outer end-wall boundary layer of a turbine than it does in a compressor. In the compressor the effect of the transverse (tangential) pressure gradient due to blade curvature is opposed by the tangentially directed shearing motion of the outer wall relative to the blade passage. In the turbine the passage curvature tends to be much larger than in a compressor, and its effect is reinforced by the tangential shearing motion of the casing relative to the blade passage. The combined effect will typically result in the formation of a vortex near the inner corner of the bend at the outer radius of the blade passage. Thus the use of Eq. (7.36) to estimate entropy generation in turbine end-wall boundary layers is likely to be more inaccurate for turbines than for compressors. Only a detailed knowledge of the link between shear stress and total velocity in the complex flow field comprised of three-dimensional boundary layers and vortex motion would allow us to evaluate \dot{S} with confidence.

A second qualitative distinction is in the relative importance of entropy generation associated with trailing-edge thickness. To keep the trailing edge of a gas turbine blade sufficiently cool to support high centrifugal stress, its thickness is typically much larger than for compressor blades. This thickness has considerable effect on the flow pattern, as Fig. 8.11 would suggest, and the wake region behind the trailing edge is an important source of loss, especially when the Mach number of the flow is high. Denton and Cumpsty [9] conclude that accurate prediction of entropy generation due to trailing-edge thickness of turbine blades will have to await further development of methods for calculating compressible viscous flows.

A third qualitative difference between compressor and turbine blades is that high-performance turbine blades are typically film cooled. There is additional entropy generation due to mixing of cooling air with the high-temperature stream of combustion products.

A fourth difference between turbine and compressor flows is that while in the former the boundary layer must be kept turbulent to prevent flow separation, there is a tendency in turbine flow passages for boundary layers—for example, on the end walls—to revert from turbulent to laminar. The Moses method (Chapter 4) of estimating turbulent boundary development shows that if the free-stream pressure falls rapidly, the boundary layer momentum thickness Reynolds number R_θ can decrease in the flow direction. In a turbine passage this decrease in Reynolds number may not be large enough for the boundary layer to revert fully to a laminar state; yet it is typically less than fully turbulent. This tends to cast further doubt on the use of Eq. (7.36) for entropy generation in turbine boundary layers. A corresponding expression [9] exists for entropy generation in laminar boundary layers, but the typical turbine boundary layer may be in between "fully turbulent" and "fully laminar."

In contrast to these extra complications for estimating entropy generation in turbine stages, there is the somewhat simplifying factor that in aircraft gas tur-

[†] Blades whose tip-radius cross sections are not connected by a circular band or "shroud."

bines (as we will see in Section 8.6) the turbine tends to operate near its design point most of the time. Also the effect of a small departure from design point operation may have less effect on entropy generation than in a compressor.

8.4 ROTOR BLADE AND DISC STRESSES

Typically the turbine blades for high-performance gas turbines are designed to avoid creep of the material during extended high-temperature operation. The allowable stress level will depend strongly on the operating temperature and may be specified as that stress which will not exceed a creep extension of, for example, 1% for 100,000 hours of operation at the temperature in question. Since 100,000 hours (11.4 years) is a long period for testing a material, it is common to see materials compared on the results of measurements of stress to cause rupture after 100 hours. Figure 8.14 from Immarigeon [10] is one such comparison. Other data have been provided by Glenny, Northwood, and Burwood-Smith [11]. We will see that for turbine blade or disc stress calculations, it is always the ratio of stress to density (the so-called strength-to-weight ratio) that is important. Hence the y-axis of Fig. 8.14 is the blade strength σ/ρ (in kPa) divided by the material density ρ (in kg/m³). Taking the density of nickel alloys to be around 8000 kg/m³ and the working temperature to be 1000°C, one sees that the σ/ρ ratio is about 20 at

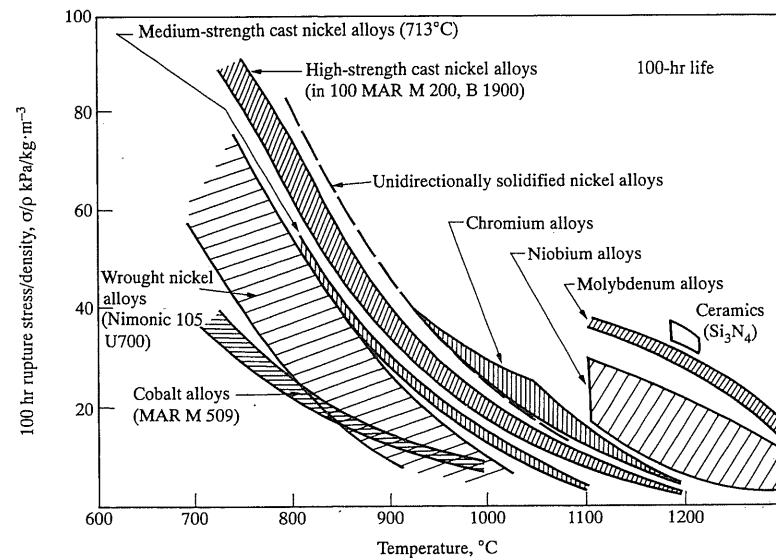


FIGURE 8.14 Variations in specific rupture strength (100 hr) with service temperature for various classes of heat-resistant materials. (Courtesy Immarigeon [10].)

most. This would imply a rupture stress of $20 \times 8000 = 160,000$ kPa, or about 23,000 lb_f/in². With a safety factor of 2, the allowable working stress would only be 80 MPa, or less than 12,000 lb_f/in². The rapid decline in strength with temperature shows the importance of the measures that have been taken in recent years to use compressor exit air to cool high-temperature blading and thus to allow gas inlet temperatures as high as 1300° to 1400°C.

Figure 8.14 shows the superior strength-temperature characteristics of ceramics. Work has been done to cast single-piece bladed turbine discs; they are cast in one piece because there is as yet no general solution to the problem of joining ceramics. Though these materials are very strong, they tend to be brittle and unreliable owing to the effect of small inclusions that severely reduce strength. There is the prospect that ceramic composites, possibly including very high strength tin whiskers, may provide a solution to the problem of how to obtain high strength along with high reliability. However, this has yet to be proved in engine practice. Alloys of chromium have limited ductility and are said to be prone to nitrogen embrittlement. Alloys of niobium and molybdenum have insufficient oxidation resistance, and they too are not used commercially in gas turbines. Cobalt-based alloys can be stronger than nickel alloys above 1050°C. They are typically more oxidation and sulfidation resistant than nickel alloys and are commonly used for turbine stator blades (nozzle vanes). The nickel-based alloys are used for highly stressed components, such as turbine blades and discs.

Grain boundaries in turbine blades tend to be the sources of weakness in materials operated at sufficiently high stress and temperature that creep is the design limitation. One way to raise turbine blade strength is to use the technique of "directional solidification," in which the blades are cast in such a way that the solid-liquid interface advances in the stress direction of the blade, allowing columnar crystals to form, aligned in that direction. Directionally solidified blades may be capable of operating at, say, 100°C, a higher temperature than with conventionally cast materials. The next step that has been taken is to cast turbine blades as single crystals, and this confers the possibility of even higher temperature operation.

Three types of stress may be of importance in various turbomachine elements: centrifugal, bending, and thermal. Centrifugal stresses are important both in blades and in the discs that support them. Bending stresses arise in the blades from the aerodynamic forces acting on them, both steady and unsteady. Thermal stresses can arise because of substantial temperature gradients within the blade that may be caused by high-intensity internal cooling.

For a given hub-tip ratio, centrifugal stress at the blade root depends primarily on blade alloy density, hub-tip radius ratio, and blade-tip speed. It is increased by blade twist, which sets up bending stress due to centrifugal loading; it can be reduced somewhat by tapering the blade cross section. Centrifugal stress is always of great concern to the designer of high-performance gas turbines. The centripetal acceleration of the center of mass of a typical turbine blade is in the range of 10,000 g to 100,000 g, so that it is not difficult to appreciate the importance of centrifugal stress in a blade whose creep strength may be greatly reduced by operation at high temperature.

Blade-root stress can also be significantly affected by the force on the blade due to the change in tangential momentum of the gas passing through the turbine rotor. As one can show by control volume analysis of the forces applied by the fluid to a turbine blade, the axial component of force is essentially equal to the difference in pressure (upstream vs. downstream of the blade row) multiplied by the annulus area and divided by the number of blades. The tangential aerodynamic force on the blade is well estimated by multiplying the total mass flow rate by the change in tangential velocity component across the blade row and, again, dividing by the number of blades. The result of such analysis shows that the gas deflection force is typically two orders of magnitude smaller than the total centrifugal force on the blade. Nevertheless, because it is applied perpendicularly to the blade rather than along its axis, it could (if the blade were sufficiently slender) set up bending stresses at the root that would be of the same order of magnitude as the centrifugal stress. The maximum bending stress will be proportional to the applied moment around the principal bending axis at the root cross section, divided by the section modulus. With this in mind one can show that for a blade of given shape (i.e., given turning angle and given thickness-to-chord ratio), the bending stress will be inversely proportional to the cube of the blade chord. Since by doubling the chord the designer can reduce bending stress by one order of magnitude, it is usually possible to maintain bending stresses at levels much smaller than centrifugal ones.

(Allowing the center of mass axis of the blade to lean slightly away from the radial direction could cause a cancellation of the root-bending stress at a given flow rate and shaft speed; the problem with this measure for an aircraft gas turbine is that at altitude the engine mass flow rate would be very much reduced, while the engine speed and turbine inlet temperature would still be high.)

The assumption implied in the foregoing is that the flow past each turbine blade is steady. As each blade passes through the wake shed by the blades of the preceding blade row, it experiences a small aerodynamic force fluctuation that could be serious if one of the critical vibration frequencies of the blade were to coincide with this wake-passing frequency. At such a resonance, destructive strain amplitudes can develop (depending on the damping available), even if the force amplitude is small. This is more likely to be a danger for slender compressor blades than for turbine blades of much sturdier cross section. It is especially serious during rotating stall (Chapter 7). Here, typically oscillating aerodynamic forces, distributed over a band of frequencies, can quickly lead to compressor blades passing through large stall zones such as may occur in surge or fatigue failure, and probably to destruction of the compressor. For turbine blades, however, stresses due to aerodynamic forces are typically much less important than stresses due to centrifugal loads.

The same is not necessarily true of thermal stresses. If blade temperature is nonuniform (as it may well be, if exposed to a gas 400° to 500°C hotter than the blade and subject to intense inner cooling through a distribution of air passages), it can suffer fairly large thermal stresses. It can be shown that at a point on the blade cross section where there is a temperature difference ΔT above or below the

mean temperature for the cross section, the local thermal stress will be about $E\alpha\Delta T$, where E is the bulk modulus for the blade material (about 2×10^5 MPa), and α is the thermal expansion coefficient (about $7 \times 10^{-6}/^\circ\text{C}$). This means that if ΔT were 50°C, the local thermal stress could be 70 MPa, or about 10,500 lb/in.², a substantial addition to the total stress. From this, one sees the importance of maintaining blade temperature uniformity. Allen [12] shows how serious thermal stresses can be in turbine blades with small internal cooling passages.

To estimate the centrifugal stresses on blades and discs, one might use Fig. 8.15 to represent one of the turbine rotors shown in, for example, the engine of Figs. 5.25 and 5.26. Taking first a cylinder of radius r that slices through the blades where their local cross sections are A_b , and defining the cross-sectional average radial stress as σ_r , we can write (for a thin section of blade dr thick in the radial direction):

$$d(\sigma_r A_b) = -(\rho_b A_b dr)\Omega^2 r, \quad (8.16)$$

in which Ω is the speed of rotation and ρ_b is the blade density. If A_b is independent of r , the equation becomes

$$\frac{d\sigma_r}{dr} = -\rho_b \Omega^2 r,$$

which may be integrated to

$$\sigma_r = -\rho_b \frac{\Omega^2 r^2}{2} + \text{const.}$$

Since $\sigma_r = 0$ at $r = r_i$, we can evaluate the constant and find that

$$\sigma_r = \rho_b \frac{\Omega^2}{2} [r_i^2 - r^2]$$

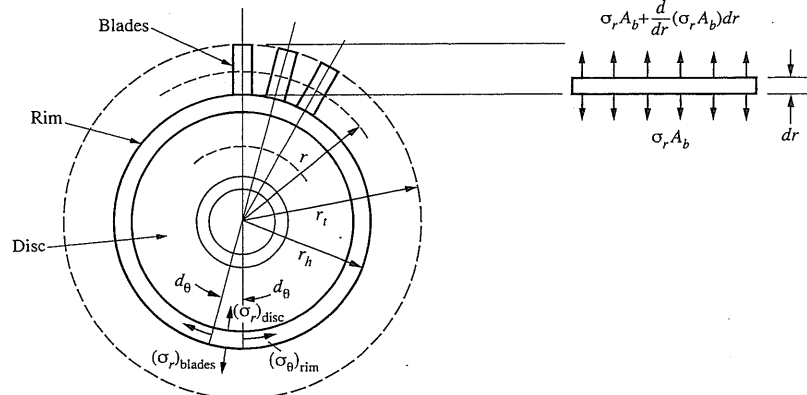


FIGURE 8.15 Turbine disc and blades.

or

$$\sigma_r = \rho_b \frac{U_t^2}{2} \left[1 - \left(\frac{r}{r_t} \right)^2 \right],$$

so that centrifugal stress at any point is proportional to U_t^2 . This can be regarded as a special case of a more general statement applicable to a rotor of any geometry that centrifugal stress will be proportional to $\rho_b U_t^2$, in which ρ_b is the material density and U_t is a characteristic (tip) speed.

The maximum centrifugal stress is located at the turbine blade hub radius ($r = r_h$) and is

$$\sigma_b = \rho_b \frac{U_t^2}{2} (1 - \zeta^2), \quad (8.17)$$

in which $\zeta = r_h/r_t$ is the hub-tip ratio. Figure 8.16 shows the maximum blade stress factor $\sigma_b/(\rho_b U_t^2)$ as a function of hub-tip ratio. In one of the problems at the end of the chapter, the effect of tapering the blade cross section so that A_b varies linearly with radius is suggested as a means of reducing σ .

We now proceed to consider the stresses in the disc that supports the blades. Bearing in mind the turbine (and compressor) disc configurations displayed in Figs. 5.25 and 5.26, we analyze, for simplicity, the disc design shown in Fig. 8.17,

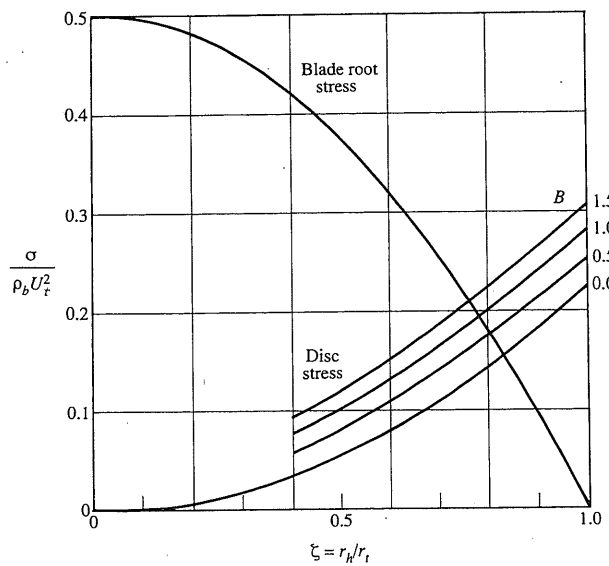


FIGURE 8.16 Centrifugal stresses with untapered blades and discs of uniform stress; $A_i/A_0 = 10$, $r_i/r_h = 0.25$.

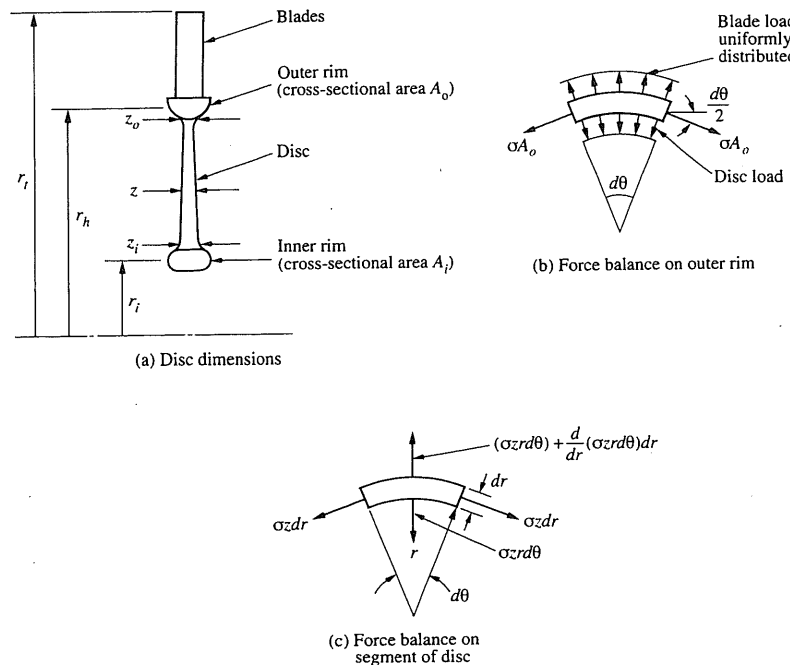


FIGURE 8.17 Disc of uniform stress with thin outer and inner rims.

which shows the upper half of a cross section of a disc consisting of two thin rims connected by a tapered disc. To make our analysis as simple as possible, we assume the following:

1. The centrifugal load applied by the blades to the rims can be considered equivalent to a radial load distributed uniformly in the circumferential direction and of the same total magnitude. (This eliminates the need to calculate circumferential variations in disc stress.)
2. The disc is tapered in such a way that its circumferential and radial stresses are everywhere equal to the same value σ .
3. The rims are thin enough that they have uniform tangential stress that, in both cases, is equal to σ . Thus the disc and both rims are “working to full capacity” with maximum allowable stress level σ throughout.
4. The discs are thin enough that we can adopt the simplified dimension scheme shown in Fig. 8.17(a). (This simplifies the algebra considerably so that we can more easily see the final results. Designers, of course, will use fairly elaborate finite-element analyses to take full account of stress concentrations, three-dimensional effects, thermal stresses, and the like. Here we

are seeking only the principal features of the effects of centrifugal loads in blades and discs.)

We begin with the force balance on the segment of the outer rim shown in Fig. 8.17(b). The radial components of forces for infinitesimal $d\theta$ are

$$2\sigma A_0 \frac{d\theta}{2} - N_b \sigma_b A_b \frac{d\theta}{2\pi} + \sigma r_h d\theta z_0 = \rho_b (A_0 r_h d\theta) r_h \Omega^2.$$

The first term is the radially inward component of the circumferential force in the rim. The second is the equivalent outward, uniformly distributed load corresponding to N_b blades for the entire circumference but here acting on only a fraction $d\theta/2\pi$ of the circumference.

The third term is the radially inward load due to the stress in the disc. The right-hand side is the mass of the rim segment multiplied by its radially inward acceleration. We assume here that the disc material density is the same as for the blades. Dividing by $A_0 d\theta \rho_b U_i^2$ and rearranging terms, we can write this equation as

$$\frac{\sigma}{\rho_b U_i^2} = \frac{\frac{N_b A_b}{2\pi A_0} \frac{\sigma_b}{\rho_b U_i^2} + \zeta^2}{1 + \frac{r_h z_0}{A_0}}, \quad (8.18)$$

in which again $\zeta = r_h/r_i$ and A_b is the cross-sectional area at hub diameter of each of the N_b blades.

Figure 8.17(c) shows the forces applied to a segment of disc of dimensions dr , $rd\theta$, and z . Here we can apply $F = ma$ again and write

$$2(\sigma z dr) \frac{d\theta}{2} - \frac{d}{dr}(\sigma z r d\theta) dr = \rho_b (dr r d\theta z) \Omega^2 r.$$

Since σ is required to be constant, we can simplify this equation (by dividing by $\sigma dr d\theta$) to

$$z - \frac{d}{dr}(zr) = -\frac{r dz}{dr} = \frac{\rho_b \Omega^2 r^2 z}{\sigma}$$

or

$$\frac{dz}{z} = -\frac{\rho \Omega^2}{\sigma} r dr,$$

which (between approximate limits $z = z_i$ at $r = r_i$ and $z = z_0$ at $r = r_h$) integrates to

$$\ln \frac{z_0}{z_i} = -\frac{\rho \Omega^2}{2\sigma} (r_h^2 - r_i^2).$$

Another way of expressing this is to write

$$\frac{\sigma}{\rho_b U_i^2} = \frac{\zeta^2 \left[1 - \left(\frac{r_i}{r_h} \right)^2 \right]}{2 \ln \left(\frac{z_i}{z_0} \right)}. \quad (8.19)$$

For the inner rim a force analysis very similar to the one for the outer rim leads to

$$\frac{\sigma}{\rho_b U_i^2} = \frac{\zeta^2 \left(\frac{r_i}{r_h} \right)^2}{1 - \frac{z_i r_i}{A_i}}. \quad (8.20)$$

Combination of Eqs. (8.18), (8.19), and (8.20) shows that we have, effectively, a disc stress function of this form:

$$\frac{\sigma}{\rho_b U_i^2} = f \left(\zeta, B, \frac{r_i}{r_h}, \frac{A_0}{A_i} \right),$$

in which the blade-loading term

$$B = \frac{N_b}{2\pi} \frac{A_b}{A_0} \frac{\sigma_b}{\rho_b U_i^2}$$

expresses the loading of the disc by the blades. Equation (8.17) (or a modification of it for tapered blades) shows how to evaluate $\sigma_b/(\rho_b U_i^2)$. The magnitude of B will typically be of order 1. With some effort the combination of Eqs. (8.18) to (8.20) can be expressed as the somewhat inconvenient function

$$\frac{A_i}{A_0} = \left(\frac{r_i}{r_h} \right) \left[\frac{B + \zeta^2 - S}{S - \zeta^2 \left(\frac{r_i}{r_h} \right)^2} \right] \exp \left\{ \frac{\zeta^2 \left[1 - \left(\frac{r_i}{r_h} \right)^2 \right]}{2S} \right\}, \quad (8.21)$$

in which $S = \sigma/(\rho_b U_i^2)$. Figure 8.16 displays typical numerical results obtained, iteratively, by using this equation to calculate S as a dependent quantity. The figure shows that whether highest stress is to be found at the blade root or in the disc depends on ζ and the other parameters. For the example given, Fig. 8.16 shows that, depending on the blade-loading parameter

$$B = \frac{N_b}{2\pi} \left(\frac{A_b}{A_0} \right) \frac{\sigma_b}{\rho_b U_i^2},$$

the disc stress can considerably exceed the blade-root stress for $\zeta > 0.7$. Aerodynamic design will tend to fix N_b , ζ , and A_b , while blade shape, as we have seen, fixes the value of $\sigma_b/\rho_b U_i^2$. Thus the only free variable affecting B is the outer rim cross-sectional area A_0 . Increasing A_0 reduces B but leads to a heavier disc. Figure 8.16 provides only an example of the use of Eq. (8.21), but we will not take further space here to discuss the determination of optimum values of A_0/A_i and r_i/r_h .

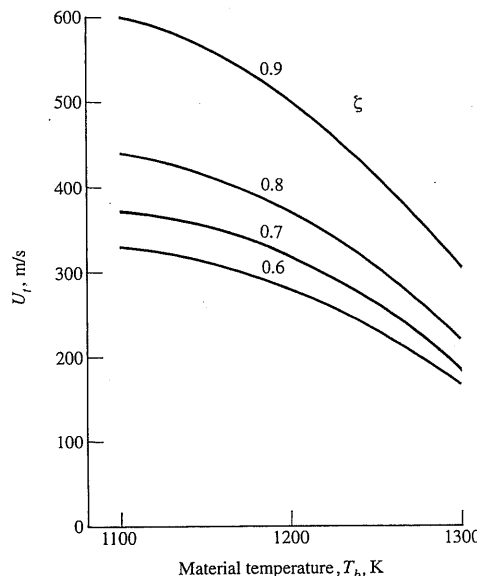


FIGURE 8.18 Allowable tip speed for various hub-tip ratios; $\zeta = r_h/r_t$.

Because the temperature of the disc can be considerably lower than the working temperature of the blades, the allowable stress on the disc can be considerably higher than on the blade; for this reason we will assume in subsequent discussion that it is blade-root stress that limits turbine design.

To see the implications of Fig. 8.14 on the allowable tip speed of turbines, we use our simplified estimate of root stress and take various values of allowable stress from Fig. 8.14 (and take the material density as 8000 kg/m^3) as a function of temperature as follows:

T/K	σ_b/MPa
1100	280
1200	200
1300	70

From these stress and density numbers one can estimate from Eq. (8.17) the allowable tip speeds shown in Fig. 8.18. We keep in mind of course that the analysis leading to these results is quite approximate and that there can be a large

difference between the temperature of the bulk of the hot gas and the blade temperature.

For typical turbojet and turbofan engines at inlet to the high-temperature section of the turbine, the gas density is sufficiently high that the hub-tip ratios are likely to be in the range 0.85 to 0.95. From the results of calculations such as the above, one might conclude that for nickel alloy turbine blades the allowable first-stage tip speed and blade temperature would be around 500 m/s and 1200 K, respectively.

8.5 BLADE COOLING

Since the maximum rotor blade stress is to be expected at the root radius of the blade, we look first at the worst case: no blade cooling and no conduction of heat away from the blade root into the turbine disc. We assume that in this case the blade temperature is nearly equal to the stagnation temperature of the hot gas (as defined for a coordinate system fixed to the blade). Given the absolute stagnation temperature T_0 (defined for a stationary coordinate system), the temperature T that would be measured upstream of the rotor at the hub radius by an observer traveling with the stream would be

$$T = T_{04} - \frac{c^2}{2c_p} = T_{04} - \frac{\gamma - 1}{2\gamma R} (c_{\theta h}^2 + c_{zh}^2)$$

or

$$\frac{T}{T_{04}} = 1 - \frac{\gamma - 1}{2} \left(\frac{U_t}{a_0} \right)^2 \zeta^2 \left[\left(\frac{c_\theta}{U} \right)_h^2 + \left(\frac{c_z}{U} \right)_h^2 \right], \quad (8.22)$$

in which the subscripts h and t denote hub and tip, respectively, and a_0 is the speed of sound at the absolute stagnation temperature T_{04} . As before, the symbol ζ indicates the hub-tip radius ratio.

The stagnation temperature relative to the coordinate system moving with the blade would be

$$T_{0\text{rel}} = T + \frac{w_{zh}^2}{2c_p}.$$

With no blade cooling or conduction into the disc, the blade would take up a temperature somewhat less than this as defined by

$$T_s = T + r_f \frac{w_{zh}^2}{2c_p}, \quad (8.23)$$

in which r_f is the “recovery” factor that accounts for the fact that the deceleration of the flow (as it enters the boundary layer next to the blade surface) is not precisely adiabatic. Some heat transfer takes place between the slowest—and therefore the hottest—streamlines and their more rapidly moving neighbors. For this reason the recovery factor is not 1 but typically in the range 0.9 to 0.95.

Combining Eqs. (8.22) and (8.23), we obtain

$$\frac{T_s}{T_{04}} = 1 - \left(\frac{\gamma - 1}{2} \right) \left(\frac{U_t}{a_0} \right)^2 \zeta^2 \left[\left(\frac{c_{\theta h}}{U} \right)^2 + \left(\frac{c_{zh}}{U} \right)^2 - r_f \left\{ \left(\frac{c_{zh}}{U} \right)^2 + \left[1 - \frac{c_{\theta h}}{U} \right]^2 \right\} \right]. \quad (8.24)$$

As an example we consider a 50% reaction blade with $c_{zh}/U = 0.5$ and $c_{\theta h}/U = 1$ (at entrance to the rotor at the hub radius) and with tip speed 500 m/s and hub-tip ratio 0.9. In this case

$$w^2 = c^2 - U^2 = c_\theta^2 + c_z^2 - c_\theta^2 = c_z^2,$$

and we find that, with $r_f = 0.9$, $\gamma = 1.33$, and $R = 0.287 \text{ kJ/kg} \cdot \text{K}$, the surface temperature T_s is 81 K below the temperature T_{04} .

Thus, even with the uncooled turbine, the rotor blade temperature at the hub, where the stress is highest, can be significantly below the "absolute" stagnation temperature of the gas at inlet to the turbine.

With blade cooling, by means of air taken from the compressor exit, it is possible to keep the blade-root temperature 300 to 400 K below the absolute stagnation temperature of the gas entering the turbine. This can be done by extraction of less than 10% of the compressor exit airflow to cool the stator and rotor blades and the turbine disc. The temperature of this cooling air depends, of course, on the compressor pressure ratio and on the flight Mach number and temperature.

More than one stage may require cooling. Even without blade cooling, gas turbines use compressor bleed air to cool the turbine disc.

The penalties of blade cooling include loss of work (and some loss of efficiency) because of that portion of the air taken from the compressor exit and ejected from the stator or rotor. In general, however, these losses are much smaller than the gains associated with operating the engine at much higher turbine inlet temperature than would be possible without cooling.

General practice in cooled turbines has been to introduce cooling air so that it exhausts through small holes on the blade surface. Figure 8.19 shows typical cooling-passage configurations in stator and rotor blading of Rolls-Royce turbines. Unlike the turbine rotor blades shown in Fig. 8.1, each of these has a platform on the outer end; the platforms of neighboring blades fit together in such a way as to create an outer ring or "shroud" at the rotor tip diameter. Shown are the separate supplies of high-pressure air—for the stator blades (nozzle guide vanes) and turbine blades—and low-pressure air for disc cooling. Figure 8.20, a turbine blade cross section, shows a five-pass internal recirculation inside the rotor blade.

Even small gas turbines are amenable to internal blade cooling using many small cooling passages. Figure 8.21 shows the blading for the General Electric T700 high-pressure rotor blades.

The question of how much airflow is required to maintain a blade at a temperature well below the gas temperature requires an estimate of heat transfer to film-cooled blades. Only an approximate estimate is possible here, but even an approximate estimate takes some care. We resort to the method outlined by

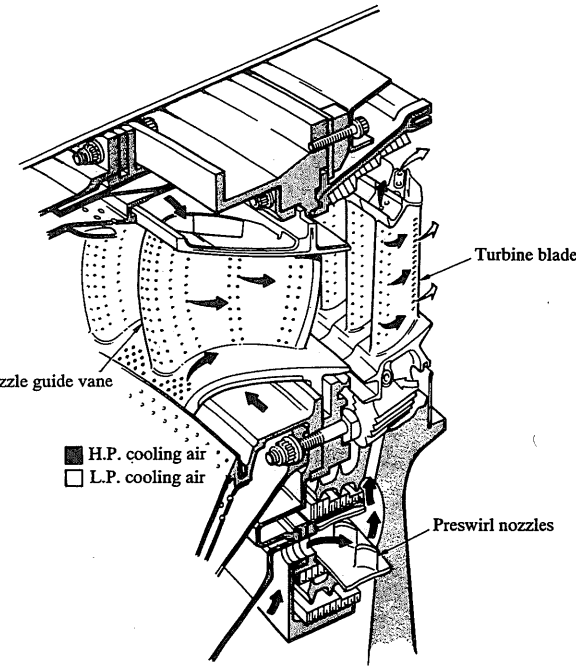


FIGURE 8.19 Cooled high-pressure turbine stage. (Courtesy Rolls-Royce, plc.)

Eckert [13], who focuses attention on a wall that is exposed on its outer surface to a hot-gas stream of temperature T_g , while the inner surface is subject to a cooling heat flux q (per unit area). At the same time, coolant air at temperature T_i is forced through holes in the walls so as to form a cooled layer of gas next to the wall, downstream of the hole. As Fig. 8.20 indicates, such cooling holes can be drilled (in production a laser drilling process may be used) at various angles relative to the cooled surface.

By reasoning with the boundary layer energy equation, Eckert shows that the heat flux from the hot gas to the wall can be written

$$q = h_0(T_{aw} - T_w), \quad (8.25)$$

in which h_0 is the film coefficient for convective heat transfer to the wall, T_w is the wall temperature, and T_{aw} is the adiabatic wall temperature. With no "film cooling"—that is, no injection of cooling air—the adiabatic wall temperature would be close, as mentioned earlier, to the stagnation temperature T_{0rel} of the gas relative to the blade surface. With coolant injection T_{aw} can be quite different

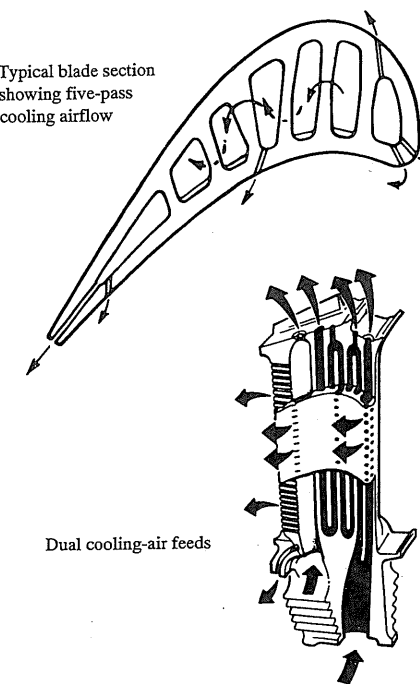


FIGURE 8.20 Five-pass cooling of turbine rotor blade. (Courtesy Rolls-Royce, plc.)

from $T_{0\text{rel}}$; we need a means of estimating T_{aw} as well as h_0 . The parameters widely used for analysis of heat transfer to film-cooled surfaces are:

1. The effectiveness η_f defined by

$$\eta_f = \frac{T_g - T_{aw}}{T_g - T_c}; \quad (8.26)$$

in which the subscript g denotes the hot-gas conditions, and T_c is the temperature of the coolant at the point of injection.

2. The Stanton number St_0 defined here as

$$St_0 = \frac{h_0}{\rho_g c_{pg} w_g}, \quad (8.27)$$

With no coolant injection the Stanton number for heat transfer to a flat plate is well known; Eckert reports that an empirically validated equation is

$$St = 0.0295 \text{Pr}^{-0.4} \text{Rex}^{-0.2}, \quad (8.28)$$

in which Pr is the Prandtl number and Rex is the Reynolds number whose length dimension is x , the distance from the leading edge of the flat plate.

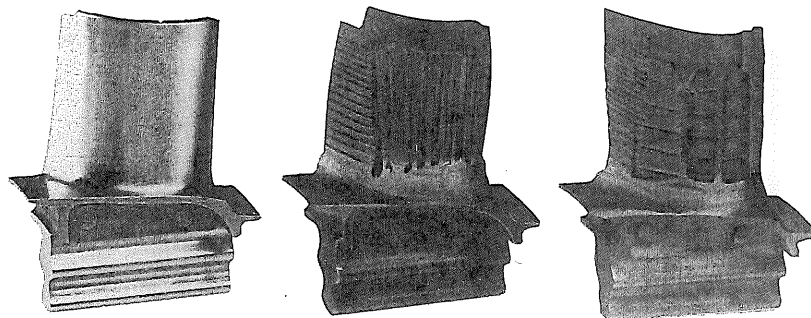


FIGURE 8.21 General Electric T700 high-pressure turbine rotor blades. (Courtesy GE Aircraft Engines.)

With coolant injection the Stanton number depends on parameters additional to Pr and Rex . The injection rate and the hole spacing are two important variables. In addition, both Stanton number and film effectiveness may be dependent on Mach number [14] (as well as on Reynolds number and Prandtl number). This dependence, however, is not very strong for typical turbine flow passages.

With film cooling, the coolant ejection hole area per unit area of surface is important; this may be written $n \pi/4 d^2$, in which d is the hole diameter and n the number of holes per unit area of cooled surface. However, n will be inversely proportional to P^2 in which P is the "pitch" or spacing between holes. Thus the coolant flow area per unit area of "porous" surface is inversely proportional to $(P/d)^2$. We can sense the importance of P/d by visualizing the spreading of the jet emitted at each coolant hole; the lateral influence of each hole will depend on the pitch-diameter ratio.

One can also expect the mass of coolant injected per unit mass of surface to be important. We can express this as

$$n \frac{\pi}{4} d^2 \rho_c u_c \propto \rho_c u_c / \left(\frac{P}{d} \right)^2,$$

in which ρ_c and u_c are the density and velocity of the injected coolant. Recognizing that P/d has separate importance (affecting the flow field in the vicinity of the holes), we can define a dimensionless "blowing parameter" as

$$M_b = (\rho_c u_c) / (\rho_g u_g)$$

and write that for film cooling on a plate

$$\eta_f, St_0 = f(\text{Pr}, \text{Rex}, P/D, M_b).$$

Typical data for effectiveness and Stanton number are shown in Fig. 8.22 for the special case $P/d = 10$ and for 11 rows of coolant in a flat plate. These data pertain to two values of the blowing parameter $M_b = 0.2$ and $M_b = 0.5$. The full line in the Stanton-Reynolds number graph represents Eq. (8.23) and shows that

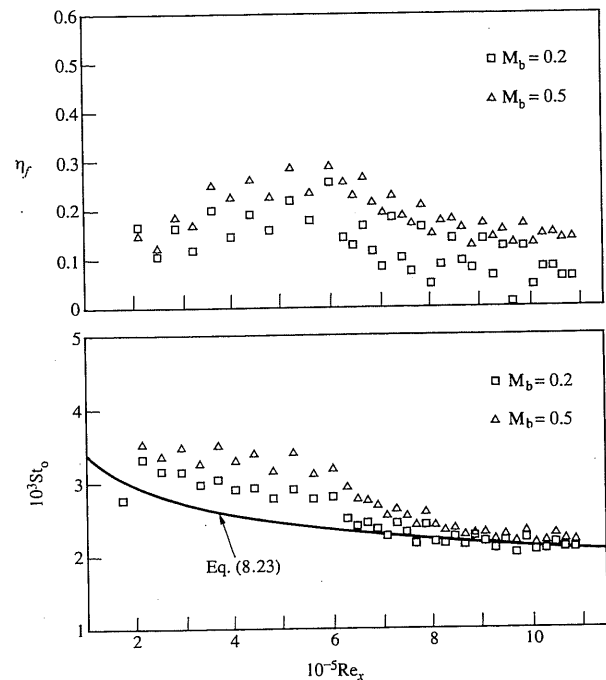


FIGURE 8.22 Effectiveness and Stanton number for a film-cooled flat-plate normal injection; $P/D = 10$. (Adapted from Eckert [13].)

coolant injection actually raises the Stanton number and thus the film coefficient of heat transfer. Nonetheless, the presence of the cool injection fluid can reduce the wall temperature.

To see the implications of these numbers for turbine blades, we assume that the blade-chord Reynolds number is 5×10^5 and that the blowing parameter is 0.5. Then from Fig. 8.22 we can take typical values for the average film-cooling effectiveness and Stanton number for the blade as

$$\eta_f = 0.2 \quad \text{and} \quad St_0 = 0.003.$$

We then suppose that these flat-plate data can be applied to the curved surfaces of an airfoil to estimate roughly the coolant flow needed to maintain a certain temperature. As the air flows up through the blade passages, we can estimate the heat transfer to it from

$$\dot{Q}_a = \dot{m}_a c_{pa} (T_c - T_i), \quad (8.29)$$

in which T_i is the temperature of the air as it is drawn off the compressor. If the heat-flow rate from blades to disc is small enough, \dot{Q}_a will be balanced by \dot{Q}_b , the

8.5 BLADE COOLING

rate of heat transfer from the hot gas to the blade surface. Using Eckert's terminology for h_0 and T_{aw} , we may estimate this as

$$\dot{Q}_b = h_0 (T_{aw} - T_b) A_s, \quad (8.30)$$

in which A_s is the surface area of the blade. To a first approximation, the required cooling-airflow rate can be obtained by equating \dot{Q}_a and \dot{Q}_b with the result

$$\dot{m}_a = \frac{h_0 (T_{aw} - T_b) A_s}{(T_c - T_i) c_{pa}}$$

or, dividing by \dot{m}_g ,

$$\frac{\dot{m}_a}{\dot{m}_g} = St_0 \frac{A_s c_{pg}}{A_g c_{pa}} \left(\frac{T_{aw} - T_b}{T_c - T_i} \right),$$

in which A_g is the hot-gas flow area (plane perpendicular to w_g).

From the definition of effectiveness

$$T_{aw} - T_b = T_g - T_b + \eta_f (T_g - T_c),$$

so that

$$\frac{\dot{m}_a}{\dot{m}_g} = St_0 \frac{A_s c_{pg}}{A_g c_{pa}} \left[\frac{T_g - T_b}{T_c - T_i} - \eta_f \left(\frac{T_g - T_c}{T_c - T_i} \right) \right]. \quad (8.31)$$

We can take here a few typical numbers to estimate the magnitude of \dot{m}_a/\dot{m}_g . Suppose:

Gas temperature	$T_g = 1600 \text{ K}$,
Blade temperature	$T_b = 1200 \text{ K}$,
Compressor exit temperature	$T_i = 850 \text{ K}$,
Coolant ejection temperature	$T_c = 1100 \text{ K}$,

and the product

$$\frac{A_s c_{pg}}{A_g c_{ps}} \approx 10.$$

Then with the value of $St_0 = 0.003$ and $\eta_f = 0.2$ we find

$$\frac{\dot{m}_a}{\dot{m}_g} \approx 0.036.$$

This estimate pertains to one rotor row. One might double this for the first stage. Cooling the second stage would not require so much air since T_g would be lower. However, from this we can see that bleeding 10% or more of compressor airflow may well be needed if high gas-inlet temperatures are used.

The use of a substantial fraction of compressor mass flow rate raises the question as to how this affects the turbine efficiency. Before we can answer this question, we must define what we mean by the efficiency of a turbine that has a number of entry points for its working fluid, each with its own stagnation pressure and temperature. It would seem reasonable in such a case to define the effi-

ciency as the ratio of the actual work to the maximum possible work of adiabatic expansion. In this case we could define, for example, the total-to-total efficiency as

$$\eta_{tt} = \frac{w_{\text{actual}}}{\sum \alpha_i \Delta h_i},$$

in which w_{actual} is the total actual work done in the turbine and Δh_i is the isentropic stagnation enthalpy drop of the i th input stream (of mass fraction α_i) expanding adiabatically by itself to the same final stagnation pressure. With the assumption of uniform and constant γ , we could write

$$\eta_{tt} = \frac{w_{\text{actual}}}{\sum \alpha_i c_p T_{01i} \left[1 - \left(\frac{p_{02}}{p_{01i}} \right)^{(\gamma-1)/\gamma} \right]},$$

in which 02 denotes the final stagnation state and 01 the initial state. Estimation of the actual stage work requires several assumptions. One might, for example, assume that the coolant stream entering the first stage does no work in that stage and mixes with the hot gas at the exit of that stage without loss of stagnation pressure. The working fluid then enters the second stage with a uniform stagnation temperature to expand adiabatically in that stage before mixing with second-stage coolant at the end of that stage. These matters are too complex to discuss in detail here, but References 13, 14, and 15 present various assumptions and procedures with which to quantify the irreversibilities associated with turbine blade cooling.

8.6 TURBINE PERFORMANCE

In Chapter 7 we saw that for any compressor the overall pressure ratio, for example, may (by dimensional analysis) be written

$$\frac{p_{02}}{p_{01}} = f\left(\frac{\dot{m} \sqrt{RT_{01}}}{p_{01} D^2}, \frac{\Omega D}{\sqrt{\gamma RT_{01}}}, \gamma, \frac{\Omega D^2}{\nu}\right),$$

in which the subscripts 01 and 02 denote inlet and outlet conditions and D is the scale or size of a series of geometrically similar machines. The Reynolds number $\Omega D^2/\nu$ is not an important variable so long as it is large enough, as we discussed earlier. The same logic as used for a compressor can be used for a turbine with the same kind of result. Thus for a given design of turbine operating with a given fluid at sufficiently high Reynolds number,

$$\frac{p_{04}}{p_{05}} = f\left(\frac{\dot{m} \sqrt{RT_{04}}}{p_{04} D^2}, \frac{\Omega D}{\sqrt{\gamma RT_{04}}}\right), \quad (8.32)$$

where stagnation states 04 and 05 are at the turbine inlet and outlet, respectively, in keeping with the scheme of Chapter 5 for numbering turbojet engines. Figure 8.23 shows the overall performance of a particular single-stage turbine. One

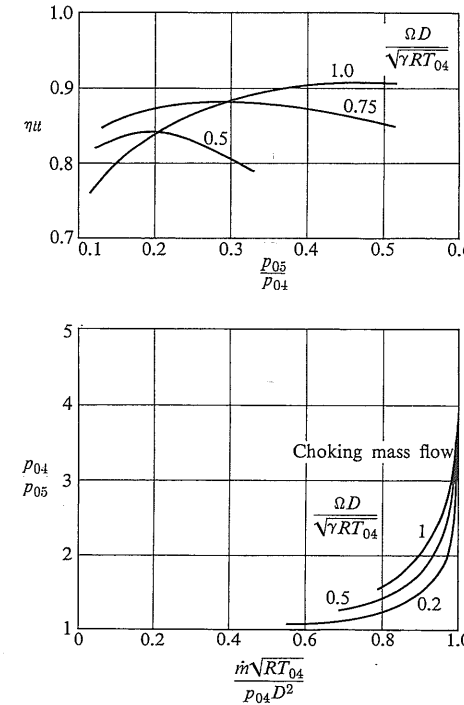


FIGURE 8.23 Typical characteristics of a single-stage free-vortex turbine. (Courtesy M.I.T. Gas Turbine Laboratory.)

can see that pressure ratios much greater than those for compressor stages can be obtained with satisfactory efficiency.

The performance of turbines is limited principally by two factors: compressibility and stress. Compressibility limits the mass flow that can pass through a given turbine and, as we will see, stress limits the wheel speed U . The work per stage, for example, depends on the square of the wheel speed. However, as Chapter 5 showed, the performance of the engine depends very strongly on the maximum temperature. Of course, as the maximum temperature increases, the allowable stress level diminishes; hence in the design of the engine there must be a compromise between maximum temperature and maximum rotor tip speed U .

For given pressure ratio and adiabatic efficiency, the turbine work per unit mass is proportional to the inlet stagnation temperature. Since, in addition, the turbine work in a jet or turboshaft engine is commonly two or three times the useful energy output of the engine, a 1% increase in turbine inlet temperature can produce a 2% or 3% increase in engine output. This considerable advantage has supplied the incentive for the adoption of fairly elaborate methods for cooling the turbine nozzle and rotor blades.

8.7 TURBINE AND COMPRESSOR MATCHING

The problem of matching turbine and compressor performance has great importance for jet engines, which must operate under conditions involving large variations in thrust, inlet pressure and temperature, and flight Mach number. Matching the components of turbofan and turboprop engines involves similar considerations and procedures, but for simplicity we focus our discussion here on turbojet engines.

Essentially the matching problem is simple, though the computations can be lengthy. The steady-state engine performance at each speed is determined by two conditions: continuity of flow and a power balance. The turbine mass flow must be the sum of the compressor mass flow and the fuel flow, minus compressor bleed flow. Also the power output of the turbine must be equal to that demanded by the compressor.

For given flight Mach number, ambient conditions, diffuser and nozzle efficiencies, and flow areas, one can determine the performance of a jet engine from the "maps" of compressor and turbine performance indicated in Fig. 8.24. These diagrams are similar to those of Figs. 7.14 and 8.23, except that, for a given machine, the constants D , R , and γ have been omitted and the speed U is replaced by the rotor rpm, N . In principle, the matching computations could proceed as follows:

1. Select operating speed.
2. Assume turbine inlet temperature T_{04} .
3. Assume compressor pressure ratio.

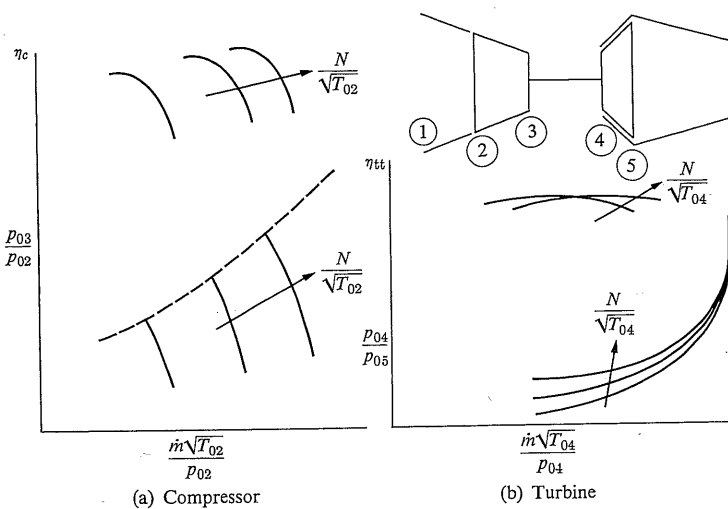


FIGURE 8.24 Typical compressor and turbine performance maps.

4. Calculate compressor work per unit mass.
5. Calculate turbine pressure ratio required to produce this work.
6. Check to see (Fig. 8.24) if compressor mass flow plus fuel flow equals turbine mass flow; if it does not, assume a new value of compressor pressure ratio and repeat steps 4, 5, and 6 until continuity is satisfied.
7. Now calculate the pressure ratio across the jet nozzle from the pressure ratios across the diffuser, compressor, combustor, and turbine.
8. Calculate the area of jet nozzle outlet necessary to pass the turbine mass flow calculated in step 6 with the pressure ratio calculated in step 7 and the stagnation temperature calculated. If the calculated area does not equal the actual exit area, assume a new value of T_{04} (step 2) and repeat the entire procedure.

The designer will try to match turbine and compressor so that the compressor is operating near its peak efficiency through the entire range of operation, as indicated in Fig. 8.25, where the operating line (i.e., the locus of steady-state matching conditions) runs through the centers of the islands defined by the constant-efficiency lines. It may happen that an operating line located in this manner will be dangerously close to the surge line. If this is the case, it might be possible to adjust the stage velocity triangles so that the maximum efficiency of the compressor occurs farther from the surge line.

Figure 8.25 is useful in a discussion of the important problem of acceleration of gas turbine engines. If an attempt is made to accelerate the engine quickly by increasing the fuel flow very rapidly, there is danger of the compressor surging, which usually causes flameout of the combustor. Also it is possible that the violent changes in aerodynamic load on the compressor blades during the surge period may cause them to fail.

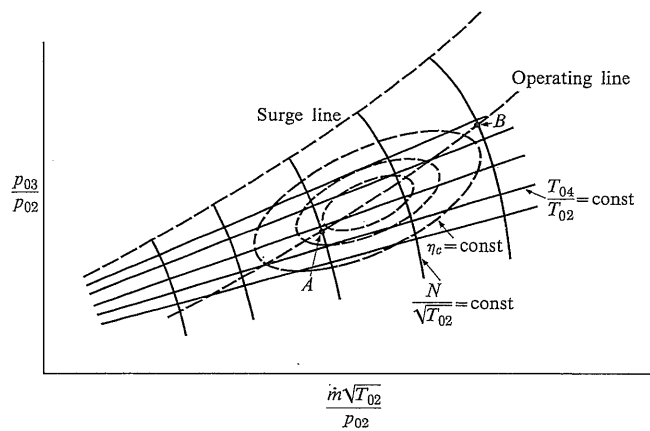


FIGURE 8.25 Operating line on a compressor map.

It is convenient to note the form of constant T_{04} lines on the compressor map. In general (referring to Fig. 8.25),

$$\frac{\dot{m} \sqrt{T_{02}}}{p_{02}} = \frac{\dot{m} \sqrt{T_{04}}}{p_{04}} \cdot \frac{p_{04}}{p_{03}} \cdot \frac{p_{03}}{p_{02}} \cdot \sqrt{\frac{T_{02}}{T_{04}}}.$$

The value of p_{04}/p_{03} is practically constant (with a value close to unity). If the turbine nozzles are choked, as they are over a good part of the operating range of turbine engines, then

$$\frac{\dot{m} \sqrt{T_{04}}}{p_{04}} = \text{const.}$$

Thus

$$\frac{p_{03}}{p_{02}} \propto \sqrt{\frac{T_{04}}{T_{02}}} \cdot \frac{\dot{m} \sqrt{T_{02}}}{p_{02}},$$

and lines of constant T_{04}/T_{02} may be plotted as shown in Fig. 8.25, straight lines radiating from the origin. Of course, at lower speeds when the turbine nozzle ceases to be choked, the lines are no longer straight.

Suppose we wish to accelerate the engine between equilibrium operating points *A* and *B*. If the fuel flow is suddenly increased, the first effect will be a sudden rise in T_{04}/T_{02} . Thus, before the rotor has time to accelerate, the compressor operation will move along a line of constant $N/\sqrt{T_{02}}$ toward the new T_{04}/T_{02} condition; that is, toward the surge line. Thus the fuel control system must limit the rate of additional fuel flow during the acceleration period. As a result, the acceleration process may be quite slow, though some engines (with variable stator blades in the compressor) can accelerate from idle to takeoff power in about six seconds, or from landing approach to full power in about three seconds.

The procedure for matching the compressor and the turbine in a turbojet engine can be much simpler, for most of the operating range, than the iterative procedure just outlined. This is because both the main propulsion nozzle and the turbine will be choked over most of the operating range. The nozzle will be choked as long as the pressure ratio across it exceeds about 2. As Fig. 8.23 shows, the turbine will also be choked when there is sufficiently high pressure across it.

Again using $\textcircled{4}$ and $\textcircled{5}$ to denote stagnation states at entrance to the turbine and main propulsion nozzle, respectively, we may write for the turbine choke condition

$$\frac{\dot{m} \sqrt{RT_{04}}}{p_{04} D^2} = \text{const}$$

and for nozzle choke

$$\frac{\dot{m} \sqrt{RT_{05}}}{p_{05} D^2} = \text{const.}$$

Dividing the first by the second, we have

$$\frac{p_{05}}{p_{04}} = \text{const} \left(\frac{T_{05}}{T_{04}} \right)^{1/2}. \quad (8.33)$$

But at the same time we can write

$$\frac{p_{05}}{p_{04}} = \left(\frac{T_{05}}{T_{04}} \right)^{\gamma/(\gamma-1)\eta_{pt}} \quad \text{or} \quad \frac{p_{05}}{p_{04}} = \left[1 - \frac{1}{\eta_{tt}} \left(1 - \frac{T_{05}}{T_{04}} \right) \right]^{\gamma/(\gamma-1)},$$

in which η_{pt} is the polytropic efficiency of the turbine expansion and η_{tt} is the total-to-total adiabatic efficiency. The only way in which these equations can all be satisfied as the engine speed and the thrust change is for both P_{04}/P_{05} and T_{04}/T_{05} to remain constant.

This has further implications. One can express the work done by a single stage in the turbine as

$$c_p \Delta T_0 = U \Delta c_\theta = U [c_z (\tan \alpha_e + \tan \beta_e) - U], \quad (8.34)$$

in which α_e and β_e signify the exit flow angles from the rotor and the stator, respectively. Even if c_z/U were to change, α_e and β_e would stay very nearly constant; as long as the blades are spaced closely enough, they can guide the flow to the same outlet flow angle regardless of small changes in the inlet flow angle, that is, in c_z/U .

If, for the moment, we consider that the turbine has only one stage, Eq. (8.34) could be written (after dividing by $c_p T_{04}$)

$$1 - \frac{T_{05}}{T_{04}} = (\gamma - 1) \frac{U}{\sqrt{\gamma R T_{04}}} \left[\frac{c_z}{\sqrt{\gamma R T_{04}}} (\tan \alpha_e + \tan \beta_e) - \frac{U}{\sqrt{\gamma R T_{04}}} \right].$$

But if that turbine stage were choked—for example, at the stator exit—it would follow that $c_z/\sqrt{\gamma R T_{04}}$ would be constant, that is, the velocity in the stage would be independent of downstream pressure and temperature. Then if γ , α_e , and β_e were also constant, it would follow that the only way T_{04}/T_{05} could be maintained constant would be for $U/\sqrt{\gamma R T_{04}}$ to remain constant. This then says that, over most of the operating range of the jet engine (as long as both the turbine and the propulsion nozzle stay choked) $U \propto \sqrt{T_{04}}$ or $T_{04} \propto N^2$, in which N is the shaft rpm. With both U and $c_z \propto \sqrt{T_{04}}$, it follows that c_z/U is constant.

If c_z/U stays constant, then (even though the turbine inlet temperature and the shaft speed vary through a wide range) all internal flow angles remain fixed. The geometry of the streamlines within the turbine does not change; the turbine may be said to be fixed at the same operating point—as defined in dimensionless terms—even though the pressure, velocity, and temperature within the turbine may vary considerably.

For a multistage turbine the argument is a little more complicated, requiring the addition of a series of equations such as (8.34) to obtain the overall tempera-

ture ratio, but the result is the same, namely, double-choking requires (as T_{04} and N change)

$$\begin{aligned}\frac{p_{05}}{p_{04}} &= \text{const}, \\ \frac{T_{05}}{T_{04}} &= \text{const}, \\ U &\propto N \propto \sqrt{T_{04}},\end{aligned}\quad (8.35)$$

and the entire turbine remains at the same (dimensionless) operating point and has the same fluid-flow angles throughout.

We now consider the consequences of the turbine remaining at the same operating point (during steady operation of the compressor-burner-turbine combination) and ask how these results control the location of the operating line shown in Fig. 8.25.

The compressor flow rate may be written

$$\frac{\dot{m} \sqrt{RT_{01}}}{p_{01} D^2} = \frac{\dot{m} \sqrt{RT_{04}}}{p_{04} D^2} \frac{p_{04}}{p_{03}} \frac{p_{03}}{p_{02}} \frac{p_{02}}{p_{01}} \sqrt{\frac{T_{01}}{T_{04}}}.$$

Since $T_{04} \propto N^2$, $\dot{m} \sqrt{RT_{04}}/p_{04} D^2$ is constant, and P_{04}/P_{03} is always close to 1; it follows that the compressor pressure ratio

$$\frac{p_{03}}{p_{02}} \propto \frac{N}{\sqrt{T_{01}}} \frac{\dot{m} \sqrt{RT_{01}}}{p_{01} D^2}. \quad (8.36)$$

Thus the operating line will have a steeper slope on the compressor map than the lines of constant T_{04}/T_{02} .

It is interesting to note that all of these results are independent of the flight Mach number of the aircraft; in terms of the compressor map there is a single operating line. If, however, the turbine or nozzle becomes unchoked—at low shaft speed—then the operating line will become dependent on flight Mach number, as shown in Fig. 8.26.

The foregoing discussion focused on the turbojet that, for a high-pressure ratio engine, is likely to have both its propulsion nozzle and its turbine choked over most of its operating range. The turbofan engine, with high bypass ratio, will typically have a much lower pressure ratio across the core engine propulsion nozzle, which may operate unchoked over part of the operating range. The bypass stream will generally be unchoked. For these conditions the simplifying considerations affecting the matching of the compressor and turbine will not apply, and one must carry out an iterative procedure for matching the compressor, fan, and turbine.

8.8 TURBINE STAGE DESIGN

In Section 7.10 we mentioned the use of two- and three-dimensional viscous compressible flow calculation procedures for compressor design. The same pro-

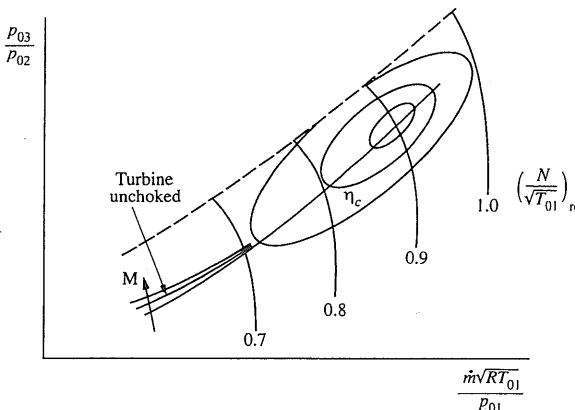


FIGURE 8.26 Operating line on compressor map.

cedures are available for turbine flows and are widely used in design and development work (see, e.g., Refs. 16 and 17). Here, as in Sections 7.9 and 7.10, we focus on more elementary methods appropriate to the preliminary design of turbine stages.

As we pointed out in Section 8.6, the dimensional analysis leading to Eq. (7.71) for axial compressors is equally applicable to compressors and turbines. Therefore we can adapt this statement of physical dependence to turbines simply by changing subscripts so that

$$\frac{p_{04}}{p_{05}}, \eta_t = f\left(\frac{\dot{m} \sqrt{RT_{04}}}{p_{04} D^2}, \frac{U_t}{a_0}, \text{design}\right). \quad (8.37)$$

The design of a turbine for a turbojet engine will be strongly affected by the compressor design as well as by the results of cycle analysis. Since the compressor is more difficult to design to high efficiency, and is generally more massive, it is the compressor that largely determines the shaft speed Ω and the maximum allowable diameter of the turbine. (Each compressor-turbine combination could theoretically have a gear transmission so that the turbine could operate on a different speed from that of the compressor, but this option appears impractical because of the mass penalty and possible unreliability of the gearbox.)

The results of cycle analysis will determine (at least approximately) the mass flow rate \dot{m} and the turbine inlet stagnation pressure p_{04} and temperature T_{04} . In addition, the design of the turbine will typically be constrained so that its maximum diameter does not much exceed that of the core compressor. However, as Figs. 5.24, 5.25, and 5.26 have indicated, the maximum diameter of the turbine is unlikely to be associated with its first stage. Thus the parameters $\dot{m} \sqrt{RT_{04}}/p_{04} D^2$

and $U_t/a_0 = \Omega D/2\sqrt{\gamma RT_{04}}$ for the first turbine stage are not rigidly determined by the results of compressor design and cycle analysis. This discussion will concern the first stage only.

In the same way as for the axial compressor, we define the preliminary design of the stage to be the determination of the overall diameter, the hub-tip ratio, the fluid-flow angles at all radii, and the blade speed ratio.

In considering the design of the first turbine stage, we could say (with reference to Eq. 8.37) that our objective is maximum pressure ratio p_{04}/p_{05} while maintaining high efficiency. Optimizing the design will mean finding values of U_t/a_0 and $\dot{m}\sqrt{RT_{04}/p_{04}D^2}$ that best satisfy the need for:

- a. A high (but not necessarily maximum) efficiency,
- b. Maximum blade-root stress consistent with the strength of available materials (e.g., Fig. 8.14) and with blade-cooling possibilities.

Stage Efficiency

Guidance on the conditions under which high turbine efficiency can be obtained is given by Fig. 8.13, which shows the wisdom of making sure that the mean-radius parameters $\Delta h_0/U^2$ and c_z/U are kept within reasonable limits. In the design process we specify the values of these parameters at the mid-radius of the stage. In addition, with high efficiency in mind, we set the mid-radius degree of reaction at 50%.

In a multistage turbine, rotor exit swirl does not necessarily imply an efficiency penalty, so zero exhaust swirl is not a requirement in the following procedure.

Blade-Root Stress

Transforming Eq. (8.17), we can write

$$\frac{2\sigma_b}{\rho_b a_0^2} = \left(\frac{U_t}{a_0}\right)^2 (1 - \zeta^2). \quad (8.38)$$

The ratio σ_b/ρ_b at which a given material may safely operate will depend strongly on the blade-root temperature, which in turn will depend on $T_{04} = a_0^2/\gamma R$ and the blade-cooling effectiveness. With turbine blade-cooling technology allowing blade temperatures to be maintained a few hundred Kelvin below T_{04} , we can deduce from Fig. 8.14 that reasonable design limits for stress can be expressed by

$$0.02 < \frac{\sigma_b}{\rho_b a_0^2} < 0.04.$$

Stagnation Temperature

As in the axial compressor, we assume that the stagnation temperature is uniform in the radial direction at each axial location in the turbine. This is consistent with radially uniform temperature at inlet to the turbine and with the work done

on each streamline being independent of radial position. In practice the flow entering the turbine will have a somewhat rounded stagnation temperature profile (lower temperature at hub and tip diameter), but we do not allow for that here.

Entropy

Again, as in the axial compressor analysis, we assume that the entropy is everywhere uniform within the stage. In this preliminary procedure we assume that the losses are accounted for by adjustments made in the stagnation pressure at exit from each blade row as the boundary layers mix with the main stream.

Radial Equilibrium

Because of high fluid density the through-flow area will be much less for the first turbine stage than for the first compressor stage. For roughly the same overall diameter we would expect the hub-tip ratio to be high. It will not be so high as to yield high efficiency without blade twist, but it will be high enough to assume that the free-vortex swirl pattern will yield a satisfactory solution to the turbine flow field.

Mass Flow Rate

As for an axial compressor stage, the mass flow rate is given approximately by

$$\dot{m} = \int_{r_h}^{r_t} \rho c_z 2\pi r dr. \quad (8.39)$$

As Section 7.8 showed, radially uniform angular momentum is compatible with a radially uniform axial velocity component. Thus the only difficulty in evaluating the integral in Eq. (8.39) is in accommodating the radial variation in density. In evaluating the integral, we have assumed that $\gamma = 4/3$. This assumption is a reasonable approximation for the specific heat ratio of the working fluid of a gas turbine; it has the additional merit of allowing Eq. (8.39) to be integrated to a closed form (as shown in Appendix VI) under the assumption of radially uniform angular momentum (i.e., a free-vortex distribution) and radially uniform entropy and stagnation temperature.

The result of the integration is a specific function in which

$$\frac{\dot{m}\sqrt{RT_{04}}}{p_{04}D^2} = f\left[\frac{U_t}{a_0}, \left(\frac{c_z}{U}\right)_t, \left(\frac{c_{\theta 2}}{U}\right)_t, \zeta\right]. \quad (8.40)$$

Here, as before, the subscript t denotes the tip diameter.

The requirement of 50% reaction at mid-radius leads (as Appendix VI shows) to

$$\left(\frac{c_{\theta 2}}{U}\right)_t = \frac{(1 + \zeta)^2}{8} \left[1 + \left(\frac{\Delta h_0}{U}\right)_m\right].$$

Also, the uniformity of c_z means that

$$\left(\frac{c_z}{U}\right)_t = \left(\frac{1 + \zeta}{2}\right) \left(\frac{c_z}{U}\right)_m.$$

Thus we can effectively consider the function represented by Eq. (8.40) to be

$$\frac{\dot{m} \sqrt{RT_{04}}}{P_{04} D^2} = f\left[\frac{U_t}{a_0}, \left(\frac{c_z}{U}\right)_m, \left(\frac{\Delta h_0}{U^2}\right)_m, \zeta\right]. \quad (8.41)$$

Work and Pressure Ratio

With constant specific heat the definition of the total-to-total efficiency of the turbine stage can be written

$$\eta_{tt} = \frac{h_{04} - h_{05}}{h_{04} - h_{05s}} = \frac{T_{04} - T_{05}}{T_{04} - T_{05s}},$$

in which 04 denotes the inlet stagnation state and 05 and 05s denote the outlet stagnation state (actual and ideal, respectively). Rearranging, we obtain

$$\frac{T_{05s}}{T_{04}} = 1 - \frac{T_{04} - T_{05}}{\eta_{tt} T_{04}}.$$

Now

$$\frac{T_{05s}}{T_{04}} = \left(\frac{P_{05}}{P_{04}}\right)^{(\gamma-1)/\gamma},$$

and at the mid-radius we may write

$$T_{04} - T_{05} = \frac{U_m (\Delta c_\theta)_m}{c_p} = \frac{U_t^2}{c_p} \left(\frac{1 + \zeta}{2}\right)^2 \left(\frac{\Delta c_\theta}{U}\right)_m.$$

Combining these expressions, we obtain

$$\left(\frac{P_{04}}{P_{05}}\right)^{(\gamma-1)/\gamma} = 1 - \frac{U_t^2}{\eta_{tt} c_p T_{04}} \left(\frac{1 + \zeta}{2}\right)^2 \left(\frac{\Delta c_\theta}{U}\right)_m$$

or

$$\frac{P_{05}}{P_{04}} = \left[1 - \frac{(\gamma - 1)}{\eta_{tt}} \left(\frac{U_t}{a_0}\right)^2 \left(\frac{1 + \zeta}{2}\right)^2 \left(\frac{\Delta h_0}{U^2}\right)_m \right]^{\gamma/(\gamma-1)}. \quad (8.42)$$

Thus, except for $(c_z/U)_m$, which does not appear in Eq. (8.42), P_{04}/P_{05} has the same independent variables as $\dot{m} \sqrt{RT_{04}}/P_{04} D^2$, and the preliminary design process can be reduced to a search for the best combination of these variables:

$$\frac{U_t}{a_0}, \left(\frac{c_z}{U}\right)_m, \left(\frac{\Delta h_0}{U^2}\right)_m, \zeta.$$

Appendix VI shows one way in which to conduct this search.

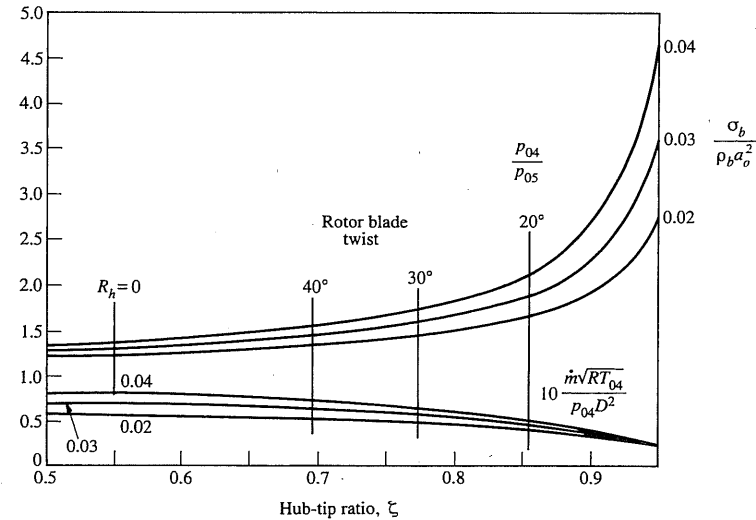


FIGURE 8.27 Axial turbine stage; $(\Delta h_0/U^2)_m = 1$ (c_z/U)_m = 0.5.

Figures 8.27, 8.28, and 8.29 show typical results of the procedure for designs for which the mid-radius degree of reaction is 50%. Figure 8.27 shows the dependence of the stage pressure ratio and mass flow rate per unit area on the hub-tip ratio for a given stress factor $\sigma_b/\rho_b a_0^2$. Taking an inlet stagnation temperature of 1600 K would give $a_0 = 801$ m/s. Referring to Fig. 8.14 and taking $\sigma_b/\rho_b = 20$ kPa/kg · m⁻³ would provide a value of $\sigma_b/\rho_b a_0^2 = 0.03$, which is in the middle of the range of values suggested earlier. If one were designing the first stage of a turbine for a turbojet, the values of P_{04}, T_{04} and the mass flow rate would be known from the results of cycle calculations. Further, design of the axial compressor would have provided a size D within which the turbine rotor should fit. Using the allowable stress parameter $\sigma_b/\rho_b a_0^2$, Fig. 8.27 would indicate the approximate hub-tip ratio of the turbine and the stage pressure ratio (for $[\Delta h_0/U^2]_m = 1$ and $c_z/U_m = 0.5$). If ζ were very close to 1, the danger would be that, with small blade height, the tip clearance losses would be excessive. On the other hand, as Fig. 8.27 shows, if the hub-tip ratio ζ were as low as 0.7 to 0.75, the rotor blade twist would become excessive. This could call for using a different swirl distribution from the free vortex on which Fig. 8.27 is based. Remember, however, that if the turbine stage were required to have zero exit swirl, the free-vortex distribution in front of the rotor is the only one that has radially uniform stage work.

As an alternative to setting the stage reaction at 50% at the mean radius, one could use the design condition that the degree of reaction be always zero at the hub radius. This would appreciably affect the calculated results. For the special case chosen (free-vortex swirl and 50% reaction at mid-radius), it is possible to

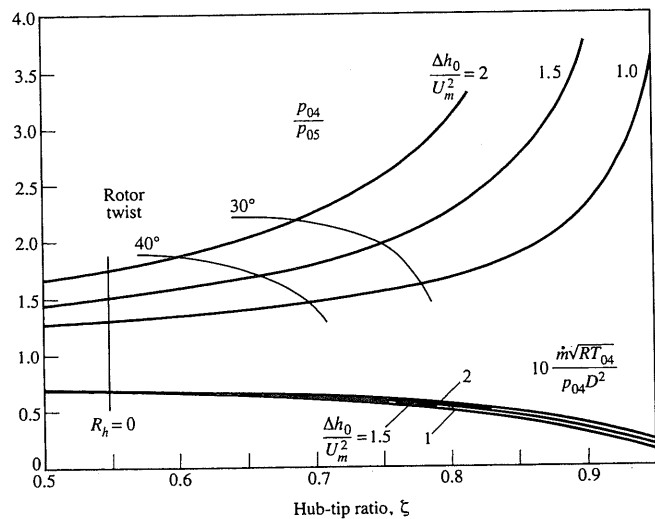


FIGURE 8.28 Axial turbine stage; $\sigma_b/p_b a_0^2 = 0.03, (c_z/U)_m = 0.5$.

show that the hub-tip ratio is always zero for a hub-tip radius ratio of 0.547. (This of course refers to the design condition; for off-design conditions the zero-degree-of-reaction point can move to a higher radius.)

Figure 8.28 shows the large effect of the work ratio ($\Delta h_0/U^2$)_m on the stage pressure ratio (and the small effect on the mass flow rate per unit area). Here we see that, for given mass flow rate parameter $\dot{m}\sqrt{RT_{04}}/P_{04}D^2$, the hub-tip ratio is not strongly affected by the work ratio.

Figure 8.29, for a given work ratio and stress parameter value, shows the effect of hub-tip ratio and flow coefficient on the overall pressure ratio and on blade twist. Raising the flow coefficient can significantly reduce blade twist; it does not under the assumed conditions affect stage pressure ratio. The higher the hub-tip ratio, the higher the allowable tip speed for a given blade-root stress; this also means higher stage work and hence a higher overall pressure ratio. Since, as mentioned earlier, the first turbine stage is likely to have a relatively high hub-tip ratio, Fig. 8.29 indicates that there will be relatively little blade twist. Thus the assumption of free-vortex swirl will be acceptable. In contrast, for the last stage of a multistage turbine, where the hub-tip ratio may be as low as 0.5, free-vortex blading could give quite unsatisfactory conditions at the blade root. Figure 8.29 indicates that the degree of reaction at the hub radius is negative for hub-tip ratios less than about 0.55 (for the chosen stage design conditions).

We have carried out this preliminary design exercise on the assumption that the radial velocity components are unimportant. Looking at the flow path of an axial turbine, however, one may see that the assumption $c_r^2 \ll c_z^2, c_\theta^2$, is not necessarily accurate. Figure 8.30, showing a low-pressure turbine, indicates that one

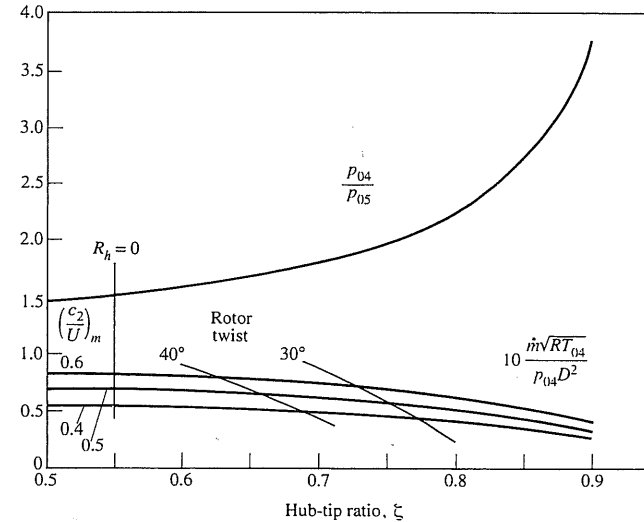


FIGURE 8.29 Axial turbine stage; $\sigma_b/p_b a_0^2 = 0.03, W/U_m^2 = 1.5$.

should take into account the radial velocity components in satisfying radial equilibrium and that a fully three-dimensional solution is needed. Procedures like those of References 16 and 17 are available to provide a good simulation of the three-dimensional flow field (except for the boundary layers) in the whole turbine.

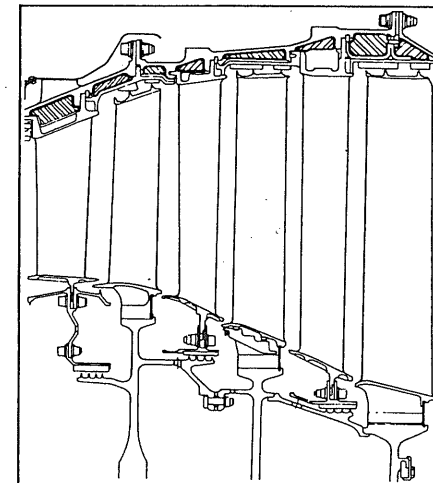
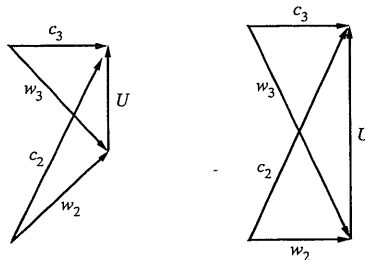


FIGURE 8.30 Low-pressure turbine flow path. (Courtesy Rolls-Royce, plc.)

PROBLEMS

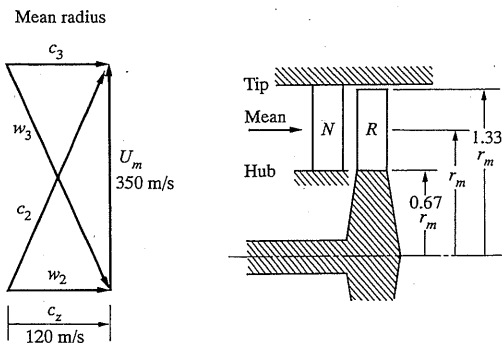
1. The figure shows velocity diagrams for impulse and 50% reaction turbines at different rotor speeds. The subscripts 2 and 3 denote conditions before and after the rotor, respectively. In both cases the absolute velocity c_2 is 400 m/s at an angle $\alpha_2 = 70^\circ$, and the absolute exhaust velocity c_3 is axial. If the blades are uncooled and well insulated from the turbine disc, approximately what would the equilibrium temperature of the blades be in each case, for an inlet gas temperature $T_{02} = 1100$ K?



PROBLEM 1

2. A single-stage axial turbine is to be designed for 50% reaction and a work ratio ($\Delta c_\theta/U$)_m of 1.0 at the mean radius. The mid-radius axial velocity ratio (c_z/U)_m is 0.4. If the swirl distribution upstream and downstream of the rotor is to be free vortex, what is the minimum hub-tip ratio for which the degree of reaction R is positive at all radii?
3. A turbine is to be designed with a "free-vortex" velocity distribution. This means that the absolute tangential velocity varies with radius according to

$$(rc_\theta)_2 = K_2, \quad (rc_\theta)_3 = K_3,$$



PROBLEM 3

PROBLEMS

where K_2 and K_3 are constants and the subscripts 2 and 3 signify the rotor entrance and exit, respectively.

- (a) Show that, with this velocity distribution, the work extracted from any unit mass of fluid flowing through the turbine is independent of radial position. (b) Construct velocity triangles (drawn roughly to scale) for the hub (r_h) and tip (r_t) velocities if the mean-radius diagram and variation of radius are as shown in the figure.

First complete the following table. Draw approximate *rotor* blade shapes at hub, mean, and tip radii.

Variable	Hub	Mean	Tip
r	$0.667r_m$	r_m	$1.33r_m$
c_z			
$c_{\theta 2}$			
$c_{\theta 3}$			

- (c) Calculate the percentage reaction [$\Delta h_{\text{rotor}}/\Delta h_{\text{total}}$] at hub, mean, and tip radii. Note that the nozzle inlet velocity is axial, so $c_1 = c_{z1} = 120$ m/sec.

- (d) What features of this design would be undesirable from boundary layer considerations?

4. An axial turbine of high hub-tip ratio runs with zero degree of reaction and peak efficiency at design flow and speed. The nozzle exit angle is 70° (from the axial direction). Estimate:

- The percentage change in torque accompanying a 20% drop in speed (from the design value) while operating with design mass flow;
- The corresponding degree of reaction.

Changes in density in the rotor may be considered negligible under design and off-design conditions. The rotor exit relative flow angle may be assumed not to vary with shaft speed.

5. An axial turbine whose hub-tip ratio is 0.57 has a flow coefficient of 0.5, a work ratio $\Delta h_0/U^2 = 1.0$, and a degree of reaction of 0.5, all at mean radius.

- If a free-vortex angular momentum distribution is used, determine the degree of reaction at the hub. Is there danger of pressure rise in the rotor?
- If a forced-vortex distribution ($c_\theta = Kr^n$) were to be adopted and the degree of reaction at the root set equal to zero, how would you determine the hub velocity triangles?

6. An axial turbine stage has an inlet temperature of 1400 K. At mid-radius, while operating at design speed and flow rate, the axial velocity ratio c_z/U is 0.5, the degree of reaction is 50% and there is no swirl in the absolute velocity leaving the rotor. The tip blade speed is 400 m/s, and the hub-tip ratio $\zeta = 0.8$.

- Estimate the stagnation pressure ratio for the stage.

- b. If, during off-design operation, the inlet flow conditions are unchanged but the speed increases 20%, show how the change in stagnation pressure ratio may be estimated. Assume that the rotor and stator exit flow angles are unchanged with departure from design conditions, and that the downstream axial velocity component does not change.

The turbine polytropic efficiency is 0.9, and the ratio of specific heat is 1.33.

7. An axial turbine (for one stage of a multistage turbine) is to be designed for a work ratio at the mid-radius of

$$\left(\frac{\Delta c_\theta}{U}\right)_m = 2$$

and a free-vortex swirl distribution upstream and downstream of the rotor. At the mid-radius the degree of reaction is to be 50%. The hub-tip ratio is to be 0.8, and the question is whether free-vortex blading would be satisfactory.

At the hub radius the stator exit angle α_{1h} is 70° to the axial direction.

- a. Draw the mean and hub velocity triangles (roughly to scale).
 - b. Determine the axial velocity ratio c_z/U_m .
 - c. Determine the rotor blade angles β_{2h} and β_{3h} at the hub radius.
 - d. Determine the degree of reaction at the hub radius.
8. An uncooled axial turbine stage is to be designed for a maximum stress at the blade root of 150 MPa (approximately 22,000 lb/in²), and the blade material density is 8200 kg/m³ (approximately 500 lb_m/ft³).

The rotor tip diameter is 0.75 m. Since the hub-tip ratio $\zeta = r_h/r_t$ is 0.9, conditions at mid-radius, where the degree of reaction is 50%, can be taken as a good average for the stage.

The turbine inlet pressure and temperature are 3.0 MPa and 1300 K (stagnation values), and the specific-heat ratio is 1.3.

If the outlet angle of the stator, at the mean radius, is 68° from the axial direction and the swirl component of the absolute velocity is zero at the stage exit, estimate:

- a. The blade-tip speed and shaft rpm;
 - b. The stage work (kJ/kg);
 - c. The pressure ratio;
 - d. The mass flow rate (kg/s).
9. At mid-radius an axial turbine stage is designed for 50% reaction, zero outlet swirl, and an axial velocity component of 200 m/s (uniform through the stage). The absolute flow angle at outlet from the stator is 65° from the axial direction.
- a. At the design point, what is the work done by the fluid at mid-radius on the rotor (kJ/kg)?
 - b. For no change from turbine design flow conditions, but with a 20% drop from design rotor rpm, estimate the work (kJ/kg) done by the rotor at mid-radius.

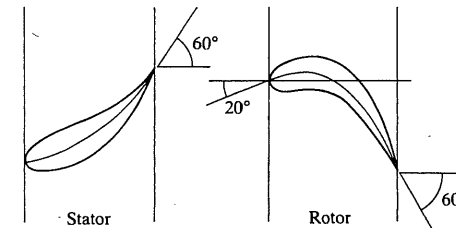
10. The stator and rotor geometry of an axial turbine is shown in the accompanying sketch for a mean-radius cross section.

- a. Establish the best operating values of:

- i. Flow coefficient $\phi = c_z/U$;
- ii. Head or work coefficient $\psi = \Delta h_0/U^2$;
- iii. Degree of reaction R .

- b. Given that the working fluid is air entering the stator at 1200 K, estimate:

- i. The stage stagnation temperature drop, for a mean blade speed of 360 m/s;
- ii. The stagnation pressure ratio of the stage.



PROBLEM 10

11. The free-power turbine of an axial gas turbine is required to produce 1000 kW, operating under the following conditions:

- i. Tip speed limited to 400 m/s;
- ii. Hub-tip radius ratio 0.6;
- iii. Inlet stagnation pressure 300 kPa;
- iv. Inlet stagnation temperature 850 K;
- v. Outlet static pressure 101 kPa;
- vi. Axial exhaust direction;
- vii. 50% reaction at mean diameter;
- viii. Axial velocity ratio 0.5 at mean diameter;
- ix. Same velocity triangles for all stages.

Determine:

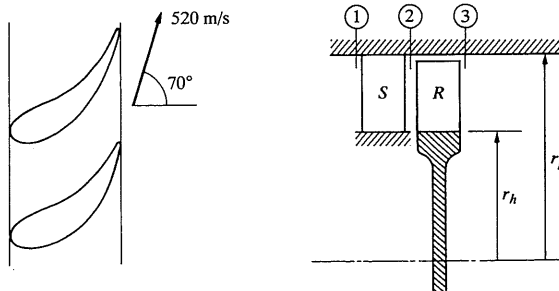
- a. The number of stages required;
- b. The rotor inlet and exit angles at the mean diameter;
- c. The stagnation temperature drops in rotor and stator.

The specific heat for the flow is 1187 J/kg · K and $\gamma = 1.333$.

12. Air leaves the nozzle of an axial turbine with a velocity of 520 m/sec at an angle of 70° with respect to the axial direction. Find the rotor blade angles

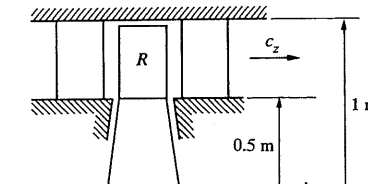
and design blade speed U such that the degree of reaction is 50% and the rotor exit swirl is zero. Assume that the blade and fluid angles are identical at inlet and outlet, respectively.

With the blade angles determined above, and the assumption that at rotor exit the relative flow angle remains equal to blade angle, show how the turbine work per unit mass varies with blade speed (i.e., at 50%, 100%, and 150% of design speed as determined above) and the same axial velocity.



PROBLEM 12

13. The flow at the exit of a turbine rotor R is swirling at "off-design" conditions. The rotor exit swirl velocity c_θ is roughly independent of radius and has a value of about 100 m/sec. The stagnation enthalpy and the entropy are also independent of radius. The gas density is approximately 1.5 kg/m^3 . Estimate:
- The static pressure difference between root and tip;
 - The axial velocity at the tip, given that it is 150 m/sec at the blade root.



PROBLEM 13

14. Show that for blades whose cross-sectional area varies linearly with radius from r_h to r_t , the average centrifugal stress at the blade-hub cross section can be expressed in the form

$$\sigma = \frac{\rho_b U_t^2}{2} \left[1 - \zeta^2 + c \left(1 - \frac{\zeta^2}{3} - \frac{2}{3\zeta} \right) \right],$$

in which

$$c = \frac{\zeta \left(1 - \frac{A_h}{A_t} \right)}{1 - \zeta}.$$

Show how with taper ratios $A_h/A_t = 0.9$ or 0.8 , the dependence of the maximum blade stress on the hub-tip ratio $\zeta = r_h/r_t$ shown in Fig. 8.16 must be modified.

15. As indicated in Section 8.4, the disc stress analysis calculation shown in Fig. 8.16(b) does not provide the results of an attempt to find optimum values for the geometric parameters of the disc. Using a spreadsheet (or another technique to facilitate iterative calculations), apply Eqs. (8.20) and (8.21) to see if the choices of r_i/r_h and A_i/A_0 ; other than those used in the calculations for Fig. 8.16, will provide lower disc stress. Consider $B = 1$ and $0.4 < \zeta < 1.0$.
16. For the control volume surrounding a single turbine rotor blade and shown in the figure, show that the tangential and axial components of blade force (per unit blade height) are given by

$$F_\theta = \rho_1 w_{z1} s (w_{\theta2} - w_{\theta1})$$

and

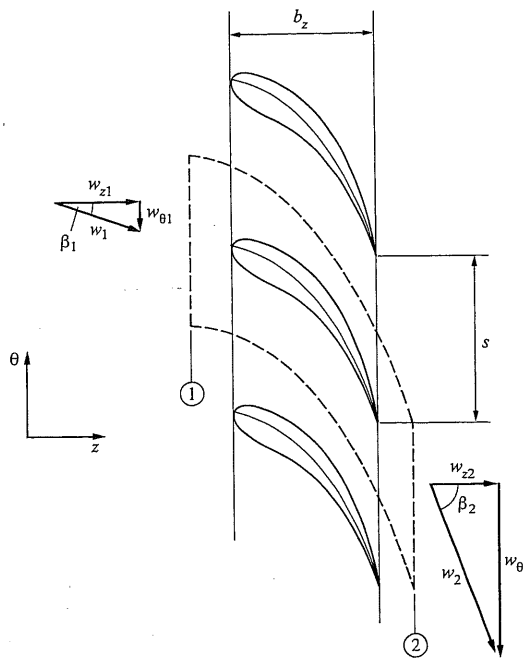
$$F_z = \rho_1 w_{z2} s (w_{z1} - w_{z2}) - s(p_1 - p_2),$$

in which s is the blade spacing and ρ_1 is the upstream density.

Defining the Zweifel coefficient as

$$Z = \frac{F_\theta}{(p_{01} - p_2)b_z},$$

show that if the flow is incompressible and $w_{z1} = w_{z2}$, the F_θ equation reduces to Eq. (8.14). If flow compressibility were allowed for, how should Eq. (8.14) be modified? Would you expect this change to be of great importance?



PROBLEM 16

17. An axial turbine stage has the hub-tip ratio of $\zeta = 0.6$. At the mean radius it has:

$$\text{Work ratio} \quad \frac{\Delta h_0}{U^2} = 1.2,$$

$$\text{Axial velocity ratio} \quad \frac{c_z}{U} = 0.6,$$

$$\text{Degree of reaction} \quad R = 0.5.$$

Two swirl distributions are being considered for the flow: One is free vortex and the other is defined by

$$rc_\theta = a(r + r_m)$$

in which r_m is the midradius.

If the stage work and stagnation conditions are radially uniform in the turbine rotor, determine the hub and tip velocity triangles for these two cases and identify the significant differences.

18. A single-stage axial turbine is designed for zero exit swirl but is called on to work at a range of flow coefficients. The mid-radius flow angle α_2 at the sta-

tor exit is specified and can be assumed to be independent of flow coefficient, as is the rotor exit relative flow angle β_3 . Show that the difference between off-design and design values of the work coefficient can be related to the flow coefficient and the nozzle (stator) flow angle by

$$\frac{\Delta h_0}{U^2} = \frac{c_z}{U} \left[\frac{\left(\frac{\Delta h_0}{U^2} \right)_{\text{design}}}{\left(\frac{c_z}{U} \right)_{\text{design}}} + \tan \beta_3 \right] - 1.$$

Regarding exit swirl kinetic energy as a loss, show how the loss ratio defined by

$$\zeta = \frac{c_{\theta 3}^2}{2 \Delta h_0}$$

varies with flow coefficient and β_3 for given values of $(\Delta h_0/U^2)_{\text{design}}$ and $(c_z/U)_{\text{design}}$.

19. A free-vortex axial turbine stage is being designed for zero exit swirl. Preliminary design calculations carried out as outlined in Section 8.8 have produced the following results in which R_h is the degree of reaction at the hub radius and twist is the absolute difference between hub and tip values of $(\beta_1 - \beta_2)$. Check whether these results are correct. The stage efficiency is $\eta_u = 0.9$ and $\gamma = 1.33$.

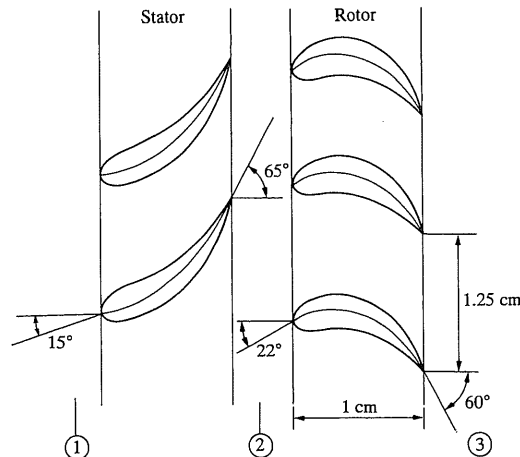
$\frac{\sigma}{\rho_b a_{01}^2}$	ζ	$\frac{\Delta h_0}{U_m^2}$	$\frac{c_z}{U_m}$	$\frac{p_{01}}{p_{02}}$	$\frac{\dot{m} \sqrt{RT_{01}}}{p_{01} D^2}$	$\frac{U_t}{a_{01}}$	R_h	Twist
0.04	0.8	1	0.5	1.316	0.0617	0.471	0.367	26.65
0.04	0.9	1	0.5	1.834	0.0415	0.649	0.443	13.11
0.03	0.8	1	0.5	1.228	0.0550	0.408	0.367	26.65
0.03	0.9	1	0.5	1.562	0.0383	0.562	0.443	13.11
0.02	0.8	1	0.5	1.145	0.0443	0.333	0.367	26.65
0.02	0.9	1	0.5	1.338	0.0333	0.459	0.443	13.11

20. In one stage of a multistage gas turbine, the blades have the mean-radius cross sections shown in the sketch.

The mean radius is 30 cm and the rotor blade height is 6 cm. At inlet to the stage the stagnation pressure and temperature are 1900 kPa and 1200 K, respectively. The absolute velocity leaving the stator is 600 m/s.

- Estimate the rotor rpm corresponding to best efficiency.
For that rotor speed determine:
 - The stage pressure ratio;
 - The tangential component of the aerodynamic force (per unit blade height) applied to one rotor blade at the mean radius.

The specific heat ratio of the gas is 1.33, and the gas constant is $R = 0.29 \text{ kJ/kg} \cdot \text{K}$. The axial velocity ratio c_z/U may be taken to be constant through the stage. Losses may be neglected.



PROBLEM 20

21. An aft-fan turbofan has the overall dimensions and main gas generator flow at sea-level static operation indicated in the figure. Stress limitations set the revolutions per minute of this assembly at 10,300 rpm. Since the original was designed, improvements in compressor blading allow fan operation at a maximum inlet absolute Mach number of 0.6 and a pressure ratio of 1.5.

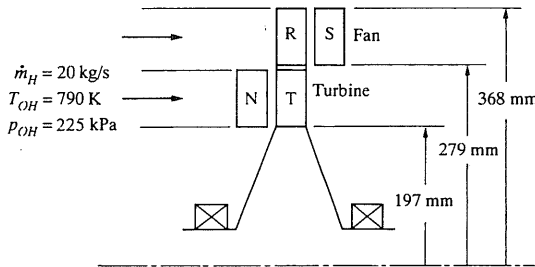
For economic reasons it is not feasible to change the radial dimensions of this element, but we wish to see what performance advantages can be gained by modifying blade shapes.

Make a preliminary design for this machine, to the extent of specifying hub, tip, and mean velocity triangles for the fan, and the mean-radius velocity triangle for the turbine. Sketch rough blade shapes (including stator and nozzle) for each velocity triangle. You may use some or all of the following design assumptions.

- Constant work from hub to tip of fan.
- No inlet guide vanes on fan.
- Axial outlet for fan and turbine.
- Constant axial velocity in fan and in turbine.
- Isentropic diffuser at fan inlet (*Note:* Compressor inlet velocity, density, and area determine fan flow rate and hence power and turbine power.)
- Ambient conditions: $p_{\text{atm}} = 100 \text{ kPa}$, $T_{\text{atm}} = 15^\circ\text{C}$, engine not moving.
- You may use $R = 0.290 \text{ kJ/kg} \cdot \text{K}$ and $c_p = 1.1 \text{ kJ/kg} \cdot \text{K}$ for both hot- and cold-gas streams.

Check the pressure coefficient at the hub and tip of both rotor and stator.

If the turbine efficiency is assumed 0.90, what is the hot-gas exhaust velocity for an isentropic hot-exhaust nozzle? If the fan efficiency is 0.85, what is the cold-gas exhaust velocity for an isentropic cold-gas nozzle?



PROBLEM 21

REFERENCES

- Kacker, S. C., and U. Okapuu. "A Mean Line Prediction Method for Axial Flow Turbine Efficiency," *Trans. ASME J. Eng. for Power* 104 (1982): 111–119.
- Smith, S. F. "A Simple Correlation of Turbine Efficiency," *J. of Royal Aeronautical Soc.* 69 (1965): 467–470.
- Moustapha, S. H., U. Okapuu, and R. G. Williamson. "Influence of Rotor Blade Loading on Aerodynamic Performance of a Highly Loaded Turbine Stage," *ASME J. Turbomachinery* 109 (1987): 155–162.
- Horlock, J. H. *Axial Flow Turbines: Fluid Mechanics and Thermodynamics*. London: Butterworths, 1966.
- Denton, J. D. "A Survey of Comparison of Methods for Predicting the Profile Loss of Turbine Blades," in *Heat and Fluid Flow in Steam and Gas Turbine Power Plant*. Inst. Mech. Engrs., (1973).
- Gregory-Smith, D. G. "Secondary Flows and Losses in Axial Flow Turbines," *Trans. ASME Series A, J. Eng. for Power* 104 (1982): 819–823.
- Sieverding, C. H. "Axial Performance Prediction Methods," in *Thermodynamics and Fluid Mechanics of Turbomachinery*, A. S. Ucer, P. Stow, and C. Hirsch, eds. Dordrecht: Martinus Nijhoff, 1985.
- Dunham, J., and P. M. Came. "Improvements to the Ainley-Mathieson Method of Turbine Performance Prediction," *Trans. ASME J. Eng. for Power* (1970): 252–256.
- Denton, J. D. and N. A. Cumpsty. "Loss Mechanisms in Turbomachines," *Proc. I. Mech. E. Int. Conf. on Turbomachinery*, Cambridge, Sept. 1–3, 1987.
- Immarigeon, J.-P. "The Super Alloys: Materials for Gas Turbine Hot Section Components," *Canadian Aeronautics and Space Institute Journal* 27 (1981): 336–354.

Reprinted with permission.

11. Glenny, R. J. E., J. E. Northwood, and A. Burwood-Smith. "Materials for Gas Turbines," *Int. Met. Rev.* 20, (1975): 1-28.
12. Allen, J. M. "Effect of Temperature Dependent Mechanical Properties on Thermal Stress in Cooled Turbine Blades," *Trans. ASME J. Eng. for Gas Turbines and Power* 104 (1982): 345-353.
13. Eckert, E. R. G. "Analysis of Film Cooling and Full Coverage Film Cooling of Turbine Blades," *Trans. ASME J. Eng. for Gas Turbines and Power* 106 (1984): 206-213.
14. Kerrbrock, J. C. *Aircraft Engines and Gas Turbines*. Cambridge, Mass.: M.I.T. Press, 1977.
15. El-Masri, M. A. "On Thermodynamics of Gas Turbine Cycles," pt. 2, *ASME J. Eng. for Gas Turbines and Power*, 108 (1986): 151-159.
16. Denton, J. D. "An Improved Time Marching Method for Turbomachinery Calculations," *J. Eng. for Power* 105 (1983): 514-525.
17. _____. "Solution of the Euler Equation for Turbomachinery Flows," pts. 1 and 2, in *Thermodynamics and Fluid Mechanics of Turbomachinery*, vol. 1, A. S. Ucer, P. Stow, and C. Hirsch, eds. Dordrecht: Martinus Nijhoff, 1985.